Nova Colinas, Maranhão State: A newly confirmed, complex impact structure in Brazil

Wolf Uwe Reimold, Ludovic Ferrière, Álvaro Penteado Crósta, Marcos Alberto Rodrigues Vasconcelos, Manfred Gottwald, Mauricio da Silva Borges, Teodoro Isnard Ribeiro de Almeida, Fernando Lessa Pereira, Ana Maria Goés, Natalia Hauser, et al.

▶ **To cite this version:**

Wolf Uwe Reimold, Ludovic Ferrière, Álvaro Penteado Crósta, Marcos Alberto Rodrigues Vasconcelos, Manfred Gottwald, et al.. Nova Colinas, Maranhão State: A newly confirmed, complex impact structure in Brazil. Meteoritics and Planetary Science, 2022, 57, pp.1519-1541. ⟨10.1111/maps.13833⟩. ⟨insu-03867006⟩

HAL Id: insu-03867006

https://insu.hal.science/insu-03867006v1

Submitted on 20 Aug 2025

HAL is a multi-disciplinary open access archive for the deposit and dissemination of scientific research documents, whether they are published or not. The documents may come from teaching and research institutions in France or abroad, or from public or private research centers.

L'archive ouverte pluridisciplinaire **HAL**, est destinée au dépôt et à la diffusion de documents scientifiques de niveau recherche, publiés ou non, émanant des établissements d'enseignement et de recherche français ou étrangers, des laboratoires publics ou privés.

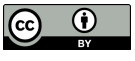

Distributed under a Creative Commons CC BY 4.0 - Attribution - International License

Check for updates

The Meteoritical Society

Meteoritics & Planetary Science 57, Nr 8, 1519–1541 (2022)
doi: 10.1111/maps.13833

Nova Colinas, Maranhão State: A newly confirmed, complex impact structure in Brazil

Wolf Uwe REIMOLD[1*], Ludovic FERRIÈRE[2], Álvaro Penteado CRÓSTA[3], Marcos Alberto Rodrigues VASCONCELOS[4], Manfred GOTTWALD[5], Mauricio da SILVA BORGES[6], Teodoro Isnard Ribeiro de ALMEIDA[7], Fernando Lessa PEREIRA[3], Ana Maria GOÉS[7], Natalia HAUSER[1], Mark JESSELL[8], and David BARATOUX[9,10]

[1]Laboratory of Geochronology and Isotope Geochemistry, Instituto de Geociências, Universidade de Brasília, Brasília, DF CEP70910-900, Brazil
[2]Natural History Museum Vienna, Burgring 7, Vienna A-1010, Austria
[3]Institute of Geosciences, State University of Campinas, R. Carlos Gomes, 250, 13083-855 Campinas, SP, Brazil
[4]Department of Geophysics, Institute of Geosciences, Federal University of Bahia, Salvador, BA, Brazil
[5]German Aerospace Center, Remote Sensing Technology Institute, 82234 Wessling, Germany
[6]Geology Faculty, Institute of Geosciences, Universidade Federal do Pará, Rua Augusto Corrêa, N° 01, Guamá, Belém, CEP: 66075-110, Brazil
[7]Institute of Geosciences, University of São Paulo, R. do Lago 562, 04280-000 São Paulo, SP, Brazil
[8]School of Earth Sciences, The University of Western Australia, 35 Stirling Hwy, Cralwry, Western Australia 6009, Australia
[9]Géosciences Environnement Toulouse, CNRS, Université Paul Sabatier Toulouse III and IRD, 14 Avenue Edouard Belin, 31 400 Toulouse, France
[10]Université Félix Houphouët-Boigny, UFR des Sciences de la Terre et des Ressources Minière, Abidjan, Côte d'Ivoire
*Corresponding author. E-mail: wolf.uwer@gmail.com

(Received 15 August 2021; revision accepted 02 May 2022)

Abstract–The Nova Colinas structure is an approximately 7 km wide, nearly circular feature centered at 07°09′33″S/46°06′30″W in Nova Colinas municipality in southwestern Maranhão State, Brazil. The area has been investigated for 40 yr and it has been suggested repeatedly that the structure could be of impact origin—without proof having been furnished. Magnetic anomaly maps depict the structure clearly with a strong, positive magnetic anomaly over the apparent rim zone. The central area is characterized by significant positive K and Th radiometric anomalies. Fieldwork showed that the structure has annular features along the outside and some prominent, structurally dissected hills in the interior. Thirty-three arenite samples were collected for petrographic analysis, mostly from within the structure. Microdeformation, in the form of cataclasis; concussion fractures related to compaction, and presence of planar fractures, feather features, and planar deformation features in quartz are reported. Three samples with a multitude of quartz grains with these microdeformations were analyzed by universal stage to determine the crystallographic orientations of planar fractures and planar deformation features. The results provide robust evidence that these microdeformation features represent shock metamorphism, with low (approximately 5–10 GPa) to moderate (10–16 and 10–20 GPa) shock levels. Thus, the Nova Colinas structure is now confirmed as a bona fide meteorite impact structure. The structure is moderately eroded, as shown by the absence of stronger shock deformation. The still limited available structural geological field evidence, paired with remote sensing and geophysical data, indicates that the innermost part of the structure may have a sizable remnant of a central uplift. The Nova Colinas impact age is only poorly constrained from stratigraphic inference to an upper limit of about 200–250 Ma.

© 2022 The Meteoritical Society.

INTRODUCTION

To date, eight meteorite impact structures have been confirmed in Brazil. In addition, a small number of other possible impact sites have been postulated in recent decades (Crósta et al., 2019a, 2019b; Gottwald et al., 2020; Kenkmann, 2021; Schmieder & Kring, 2020). One of these possible impact sites is a structure originally known as the Macapá Structure (Abreu et al., 1977). This remarkable landform is centered at 07°09′33″S/46°06′30″W, in the municipality of Nova Colinas (population approximately 5350), in southwestern Maranhão State, in an area known as the Chapada das Mangabeiras, north of the town of Balsas (Lima, 1995) (Figs. 1 and 2a). The structure has a diameter of approximately 7 km. The name "Macapá" was derived from the Macapá River that transects the center of the structure from west to east. In the previous literature, several hypotheses were proposed to explain the "Macapá Structure," including impact cratering, the intersection of fracture systems, or a structural basin (see e.g., Barbosa da Silva, 2020).

Barbosa da Silva (2020) referred to this enigmatic structure as Cabeça de Sapo (Portuguese, Toad's Head), a name credited to S.L.A. Brenha of the Federal University of Maranhão (Brenha, 2013; de Oliveira, 2017). A circular aeromagnetic anomaly over this structure was noted in a survey conducted by the Brazilian National Petroleum Agency (ANP) (Marques et al., 2006). The earliest published notion that the structure could be of impact origin seems to stem from

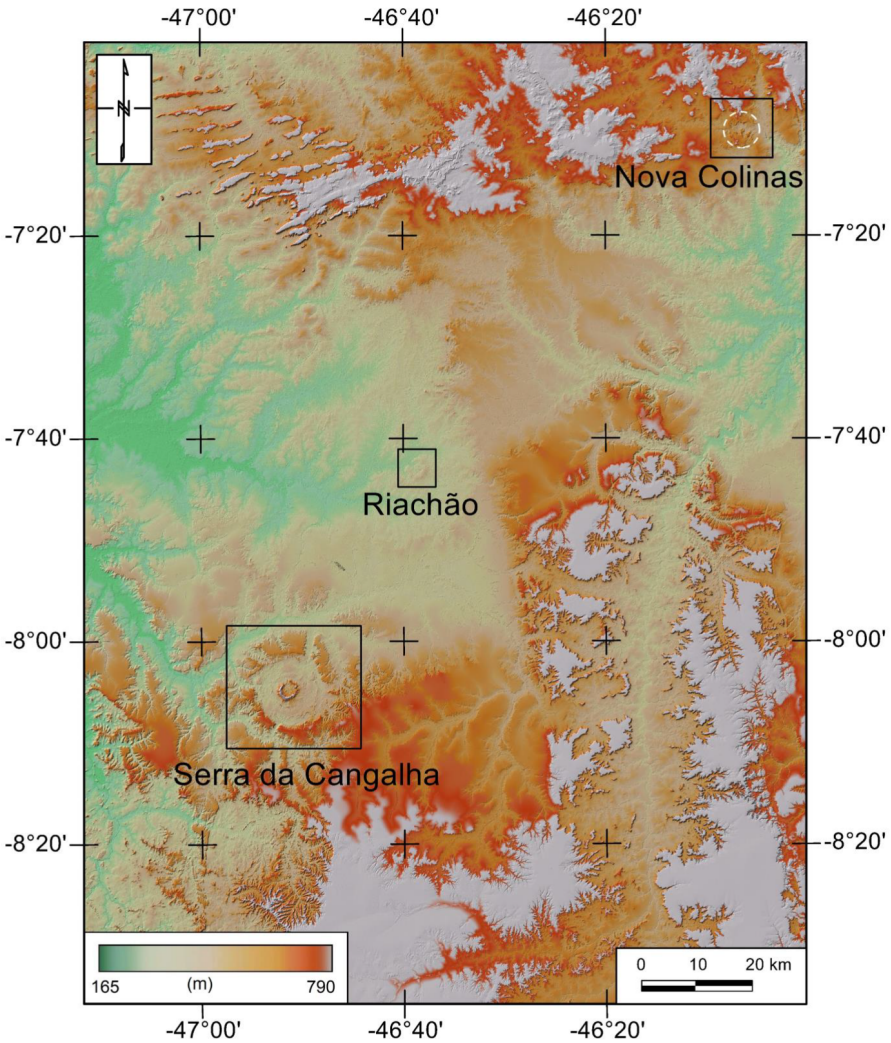

Fig. 1. TanDEM-X topographic map for the southern part of the Parnaíba Basin in the southwest of Maranhão, and far northeast of Tocantins, states of Brazil, showing the locations of the two confirmed impact structures of Serra da Cangalha and Riachão, in relation to the location of the Nova Colinas structure (in the northeasternmost section of this image). Note that the three structures are not strictly aligned—the Nova Colinas structure is visibly offset to the east from the trend defined by the locations of Serra da Cangalha and Riachão. (Color figure can be viewed at wileyonlinelibrary.com.)

19455100, 2022, 8, Downloaded from https://onlinelibrary.wiley.com/doi/10.1111/maps.13833 by Cochrane France, Wiley Online Library on [20/08/2025]. See the Terms and Conditions (https://onlinelibrary.wiley.com/terms-and-conditions) on Wiley Online Library for rules of use; OA articles are governed by the applicable Creative Commons License

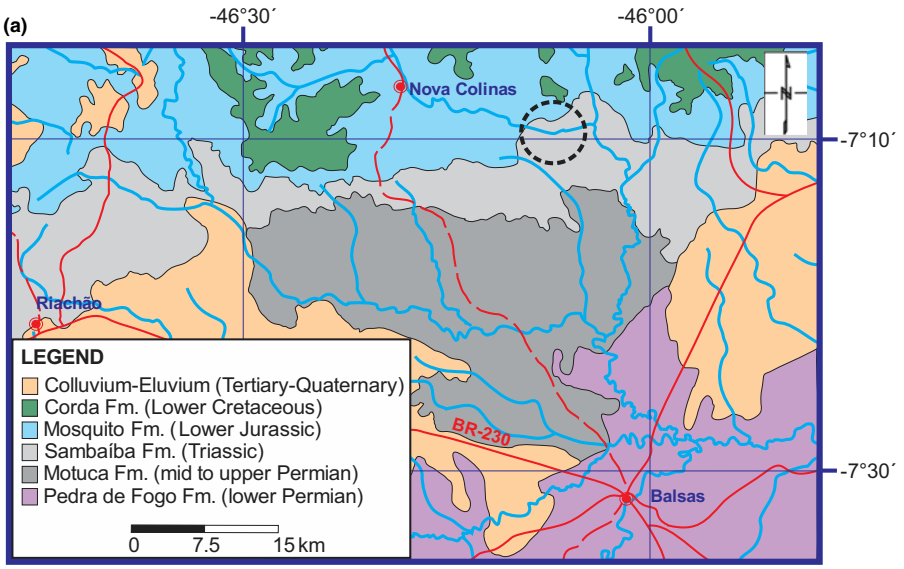

(b)

PERIOD	FORMATION	DESCRIPTION	NNW DISTRIBUTION SSE	T[m]
LOWER CRETACEOUS	CORDA	Fine-grained sandstone with medium-scale cross-bedding (1),fine-grained sandstone with parallel bedding (2), and medium- to coarse-grained sandstone with medium-scale trough cross-bedding (3).		30
LOWER JURASSIC	MOSQUITO	Basalt with intercalations (intertrap) of poorly-sorted sandstone lenses.	Sandstone lenses	190
TRIASSIC	SAMBAÍBA	Fine- to medium-grained sandstone with large-scale cross-bedding.		440
	MOTUCA	Red laminated mudstone interbedded with fine-grained sandstone and evaporite lenses.	Evaporite levels	140
PERMIAN	PEDRA DE FOGO	Reddish brown mudstone with frequent intercalations of chert and sandstone levels.	Chert levels	240

Fig. 2. a) Schematic geological map of the region between the Nova Colinas and Riachão structures (modified from the 1:750,000 geological map of Maranhão State—Klein & Souza, 2012). Note that the original CPRM map indicates an "Estrutura de Impacto," but that they placed this feature further to the southwest of the actual site shown here. The Nova Colinas structure lies close to the southern limit of the Mosquito Formation area. b) Stratigraphic chart of the Paleozoic and Mesozoic units of the region around the Nova Colinas and Riachão impact structures. The column is based on the work of Vaz et al. (2007), Andrade (2019), and Nogueira et al. (2021). T = thickness in meters, E = eolian dune field deposits, L = lacustrine deposits, L/P = lacustrine/playa deposits, F = fluvial deposits, and S = sand sheet deposits. (Color figure can be viewed at wileyonlinelibrary.com.)

19455100, 2022, 8, Downloaded from https://onlinelibrary.wiley.com/doi/10.1111/maps.13833 by Cochrane France, Wiley Online Library on [20/08/2025]. See the Terms and Conditions (https://onlinelibrary.wiley.com/terms-and-conditions) on Wiley Online Library for rules of use; OA articles are governed by the applicable Creative Commons License

the regional geological map of Maranhão State by the Geological Survey of Brazil (CPRM, 2012; Klein & Souza, 2012) and IBGE (Instituto Brasileiro de Geografia e Estatística, 2011). More recently, Barbosa da Silva (2020) pointed out the possibility of impact origin in his analysis of aerogeophysical and remote sensing data—although without providing any diagnostic evidence to support this hypothesis.

Here, we introduce the name Nova Colinas for this structure that is located within the territorial limits of the homonymous small town a few kilometers to the northwest. The previous reference to a "Macapá" structure is related to the extensive stream feature that transects the structure. However, this name is well known in Brazil as the designation of the capital city of Amapá State in northeastern Brazil located more than 970 km to the northwest of the structure discussed here. In order to avoid misunderstandings, we prefer the name Nova Colinas, as it relates the local structure directly to a local landmark in the southern part of Maranhão State (cf. Fig. 2a).

The Nova Colinas (NC) structure comprises a central lowland interspersed with isolated hills or short ranges of moderate elevation (300–400 m), all of which are surrounded by prominent ridges. The approximately 7 km diameter of the structure, defined by the outer ridges likely representing the crater rim zone, has been measured from satellite imagery (e.g., de Oliveira, 2017; Gottwald et al., 2020). The area is partially utilized for agriculture, with remnants of native forest and savanna (cerrado), and riparian vegetation. Nova Colinas is located relatively close to two other confirmed impact structures, Riachão at about 80 km and Serra da Cangalha at 135 km to the southwest (Fig. 1; for detail about these other structures, see Crósta et al. [2019a] and references therein). It has been suggested in the past that these three structures were well aligned and could be of common origin. However, Fig. 1 illustrates that Nova Colinas deviates significantly (by approximately 20 km) from proper alignment with the other two structures.

Here, we present detailed analysis of satellite sensor and geophysical data sets, as well as results from a reconnaissance 5-day field survey in September 2019. This field visit allowed us to obtain a first overview of the geology and collect a large number of samples for shock petrography. The shock petrographic results leave no doubt that the Nova Colinas structure represents a bona fide impact structure.

Regional Geology

The Nova Colinas, Riachão (Mazivieiro et al., 2013), and Serra da Cangalha (Kenkmann et al., 2011; Vasconcelos et al., 2013) impact structures are located in the central part of the 600,000 km^2 Parnaiba Basin (Figs. 1 and 2a). This intracratonic basin involves a predominantly siliciclastic, up to 3.5 km thick sedimentary pile deposited above Precambrian crystalline basement (e.g., Brito Neves et al., 1984; Cordani et al., 2009). The sedimentary sequences are divided into the Silurian-Lower Devonian Serra Grande Group, the Middle Devonian to Lower Carboniferous Canindé Group, the upper Carboniferous to Triassic Balsas Group, and Jurassic and Cretaceous sequences of the Mearim Group (Góes & Feijó, 1994).

The Mosquito Formation of the Mearim Group (Ballén et al., 2013; Góes & Feijó, 1994; Vaz et al., 2007) represents volcanic strata formed during the opening of the Central Atlantic Ocean around 190 Ma ago. The Mosquito Formation is related to the Central Atlantic Magmatic Province (CAMP; Marzoli et al., 2018). In the study area, Merle et al. (2011) obtained ages for Mosquito lavas from 199.7 ± 2.4 Ma to 197.2 ± 0.5 Ma by the ^{40}Ar-^{39}Ar method; thus, these rocks are of Lower Jurassic age.

In contrast, the sills and dikes of intrusive rocks of the 130 Ma Sardinha Formation occur strictly on the eastern edge of the Parnaíba Basin. This magmatic event is associated with the opening of the Southern Atlantic Ocean, possibly related to the Lower Cretaceous Paraná-Etendeka Large Igneous Province (Góes & Feijó, 1994; Oliveira et al., 2018). Several authors have referred to the likely occurrence of dolerite dikes in the area of interest around Nova Colinas, presumably associated with the volcanics/subvolcanics of the Mosquito Formation (e.g., Barbosa da Silva, 2020).

The area of the NC structure can be broadly divided into two parts of contrasting geology (according to Klein & Souza [2012]—1:750,000 geological map of Maranhão State—Fig. 2a). The northern part of the structure involves the southernmost extension of the Jurassic basalts of the Mosquito Formation, which are locally overlain by Lower Cretaceous sandstones of the Corda Formation (also compare fig. 2 of Ballén et al., 2013; fig. 9 of Barbosa da Silva, 2020, adapted from Ferreira, 2013; and our geological photointerpretation in Fig. 3b). In contrast, the central and southern sectors of the area seem to be dominated by Triassic sandstones of the Sambaíba Formation and Middle to Upper Permian red mudstones with intercalations of sandstones and evaporites of the Motuca Formation (Góes & Feijó, 1994; Santos & Carvalho, 2009; Vaz et al., 2007). The lower Permian Pedra de Fogo Formation (red mudstones interbedded with many chert levels) occurs mainly to the south of the structure but, based on the available regional geological information, it appears possible that these

19455100, 2022, 8, Downloaded from https://onlinelibrary.wiley.com/doi/10.1111/maps.13833 by Cochrane France, Wiley Online Library on [20/08/2025]. See the Terms and Conditions (https://onlinelibrary.wiley.com/terms-and-conditions) on Wiley Online Library for rules of use; OA articles are governed by the applicable Creative Commons License

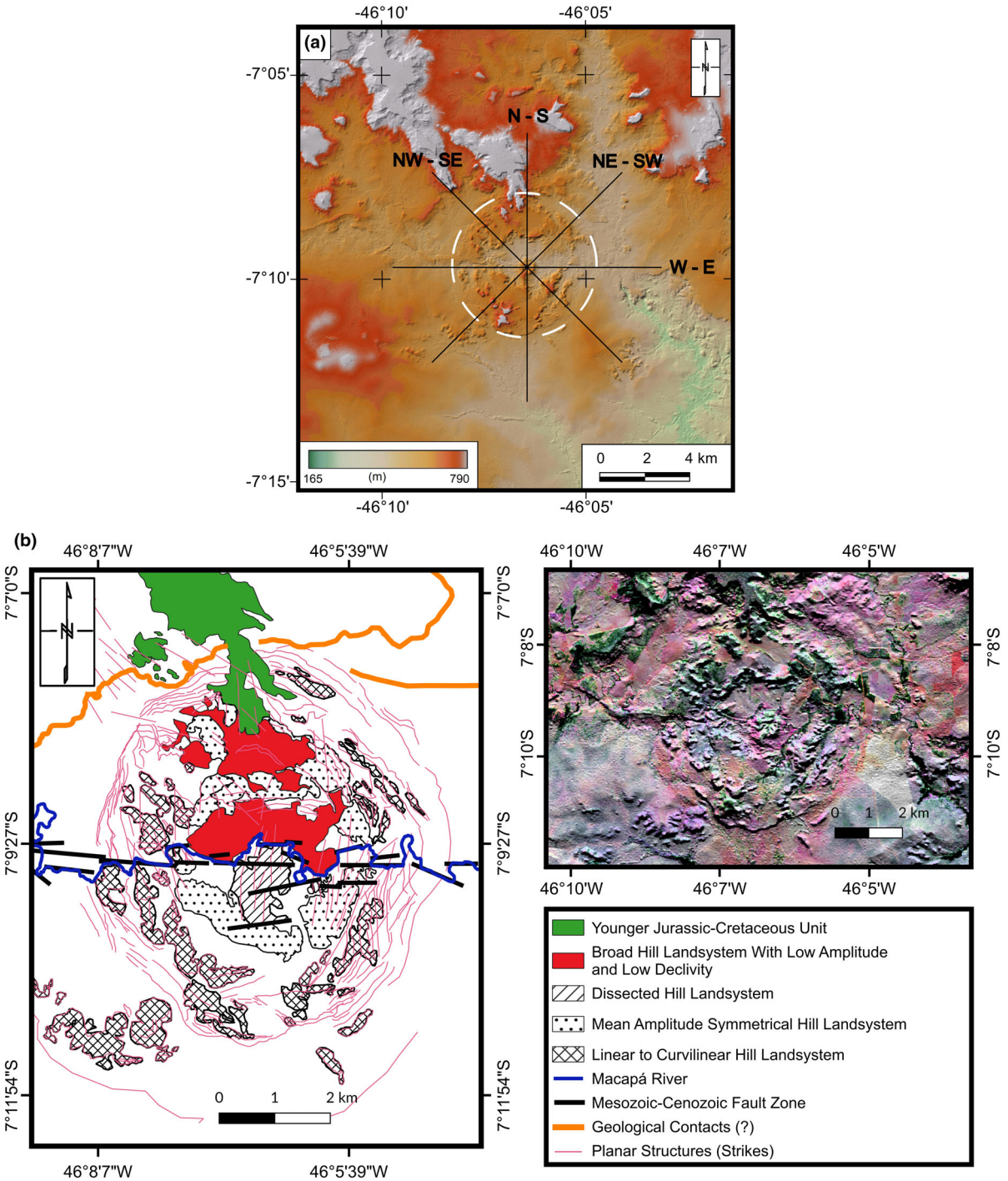

Fig. 3. a) Digital elevation model (DEM) of the Nova Colinas structure produced from TanDEM-X data. The locations of the elevation profiles extracted from this DEM (Fig. SM-3d, supporting information) are indicated. b) Geological interpretation of a scene generated from Sentinel-2 (channels 2,3,4) data fused with a 5 m spatial resolution China–Brazil Earth Remote Sensing Satellite (CBERS-4) panchromatic image (upper right, above legend), and also based on ground-based information from site visits by MB and students from the Federal University of Pará (Belém) between 1989 and 1994. c) Sun-shaded TanDEM-X scene for the Nova Colinas structure, with sampling sites and first structural data (for bedding orientation data, compare Table SM-2, supporting information) from the September 2019 site visit by WUR and MARV. Note that, in this map, the site locations are given as degree + minute values, whereas in Table SM-2, the values are listed in decimal version. The inset refers to the location of the Nova Colinas structure in Brazil, and the red dot represents the location of the city of Brasília, for reference. Fazenda do Nem is located in the low-lying, northwestern area of this TanDEM-X scene. (Color figure can be viewed at wileyonlinelibrary.com.)

19455100, 2022, 8, Downloaded from https://onlinelibrary.wiley.com/doi/10.1111/maps.13833 by Cochrane France, Wiley Online Library on [20/08/2025]. See the Terms and Conditions (https://onlinelibrary.wiley.com/terms-and-conditions) on Wiley Online Library for rules of use; OA articles are governed by the applicable Creative Commons License

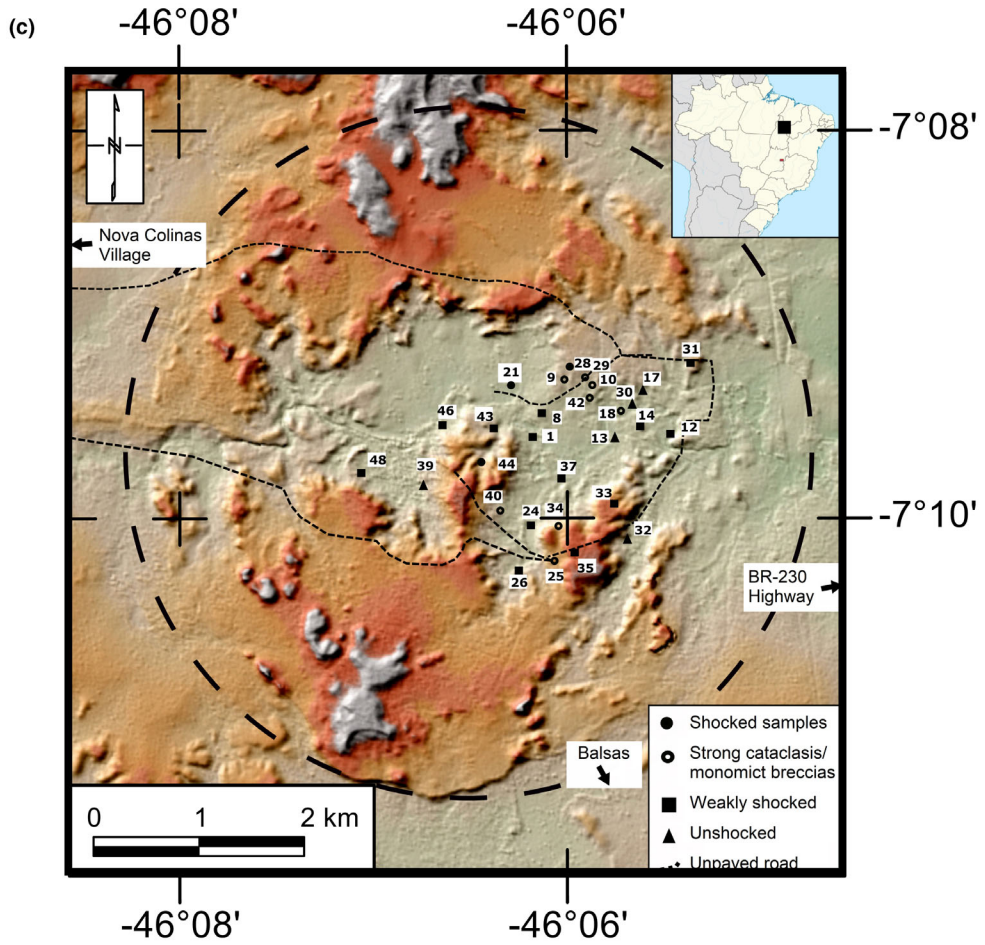

Fig. 3. Continued.

strata may just occur still at the southeastern limit of the Nova Colinas structure, or possibly within it. The stratigraphic relationships of the Paleozoic and Mesozoic units outcropping in the region surrounding the Nova Colinas and Riachão structures are schematically presented in Fig. 2b.

Previous Geophysical Work

The first geophysical analysis of impact structures in the Parnaíba Basin was presented by Vasconcelos et al. (2010), who pointed out the occurrence of four potential structures: Serra da Cangalha, Riachão, Santa Marta, and São Miguel do Tapuio. They showed that the first three of these structures exhibited gravimetric and magnetic signatures that would be considered typical of impact structures in similar geological settings, whereas São Miguel do Tapuio did not show an unequivocal signature. Later, all four structures were proven to be of impact origin (see review by Crósta et al., 2019a, 2019b). In the case of the Nova Colinas structure, aerogeophysical and remote sensing data were used by Barbosa da Silva (2020) to suggest a possible impact origin.

Barbosa da Silva (2020) reported new interpretations of magnetic and radiometric anomaly maps. The former indicated a strong ring-shaped, positive anomaly over the apparent rim of the structure. From the northern rim outward, a strong, rough, positive anomaly is also indicated and was interpreted to correspond to basic volcanics of the Mosquito Formation. In the airborne gamma ray spectrometric results, this author referred to ring-shaped anomaly patterns, but these are hardly recognizable in his imagery. There is, however, an indication of slightly positive K, Th, and U anomalies in the innermost sector of the structure. Profiles based on an ALOS/PALSAR digital elevation model (DEM) indicated an area in the innermost part of the structure that is elevated by approximately 40 m over the more external parts of the structure's interior. Barbosa da Silva (2020) suggested that this could represent a central uplift structure—without providing any direct evidence.

19455100, 2022, 8, Downloaded from https://onlinelibrary.wiley.com/doi/10.1111/maps.13833 by Cochrane France, Wiley Online Library on [20/08/2025]. See the Terms and Conditions (https://onlinelibrary.wiley.com/terms-and-conditions) on Wiley Online Library for rules of use; OA articles are governed by the applicable Creative Commons License

METHODS

Field Access

Access to the Nova Colinas structure can be achieved either from the town of Riachão via secondary and tertiary roads toward the small, rural town of Nova Colinas located some 17 km (by road) west–northwest of the structure. A further gravel road reaches the northern rim of the structure, skirts it toward the northeast, and then enters into the structure. Alternatively, coming from the regional hub Balsas, the structure is reached via the MA-006 state road and then joining the BR-230 secondary road, from where a dirt road connects with the structure on its eastern side.

Satellite Imagery

The suite of spaceborne remote sensing data used to characterize the structure includes images from several multispectral sensors, specifically Landsat Thematic Mapper/Enhanced Thematic Mapper+ (TM/ETM+), Advanced Spaceborne Thermal Emission and Reflection Radiometer (ASTER), and Copernicus/Sentinel-2B, all with spatial resolution between 60 and 10 m. The multispectral bands of these sensors were used to generate color composite images, spatially enhanced by the panchromatic band (5 m spatial resolution) of the China–Brazil Earth Remote Sensing Satellite (CBERS-4/Pan) or by the ETM+ panchromatic band (15 m spatial resolution).

The multispectral remote sensing data for the Nova Colinas region were also exploited with a novel geobotanical approach for obtaining information possibly related to the different lithologies of NC, based on vegetation types and seasonal variations. This method assumes that, to a certain extent, bedrock types influence the biota that grow in soils above it, particularly when considering seasonal variations. In tropical/subtropical environments with large biodiversity, small changes in the local geology may reflect local phytosociology (Tuomisto et al., 2003, in the Amazon's Terra Firme rainforest; Almeida et al., 2007, in the Atlantic rainforest of SE Brazil; Almeida et al., 2019, in the Pantanal Biome). These changes are enhanced when comparing vegetation indices and thermal responses using remote sensing data obtained in humid and dry seasons.

The cerrado (the Brazilian savanna) is one of the most diverse vegetation types, second only to tropical rainforests (Eiten, 1994). This type of vegetation dominates the landscape of southern Maranhão. Cerrado has a large range of xeromorphic species, from deciduous to evergreen, but predominantly semideciduous, species. For the selection of Landsat/ETM+ images depicting seasonal vegetation differences, we used weather data from the nearby meteorological station in Balsas, 51 km to the SE of the NC structure. Suitable cloud-free images were selected for September 1, 1999, as well as May 14 and August 18, 2000. As the aim was to test the spatial–temporal variability of surface temperature (using emissivity in the thermal infrared) as an ecological indicator, we selected this sensor due to its better spatial resolution (60 m) than that of other satellites with thermal capabilities. A panchromatic band with a higher spatial resolution (15 m) of the same sensor from the August scene was used to better depict the spatial variability. To complement the analysis of the multitemporal thermal images, we used a normalized index, NDWI (Normalized Difference Water Index), proposed by Gao (1996), which registers leaf water content. This application of the geobotanical approach to Nova Colinas is, to our knowledge, the only one dealing with an impact structure.

Digital Elevation Model

Satellite-based DEMs provide a valuable asset to investigate potential sites of candidate impact structures and also to characterize the surface features of candidate and confirmed impact structures. Where an original crater has been partially modified by subsequent geological processes (e.g., erosion, sedimentation, partial burial), a DEM can also support its characterization by providing important textural/structural information. According to Gottwald et al. (2017, 2020, 2021), a DEM with enough spatial resolution can provide detailed information on the morphology of an impact structure, yield insight into the local and regional topographic context, and facilitate the planning of field surveys. Among the existing spaceborne global DEM data, the TanDEM-X offers the best spatial resolution (12 m) (Gottwald et al., 2021, their table 2). The TanDEM-X experiment used two satellites operating in tandem mode to generate global interferometric elevation data, with an unprecedented spatial resolution, an absolute horizontal and vertical accuracy of <10 m, and relative vertical accuracy of 2–4 m, depending on how mountainous the terrain is (2 m for flatter, and 4 m for mountainous, terrain).

Geophysical Data and Processing

We employed the same data used by Barbosa da Silva (2020), acquired and preprocessed in 2005 and 2006 by ANP. The data consist of gamma ray and magnetic data, with 500 m-spaced north–south flight

19455100, 2022, 8, Downloaded from https://onlinelibrary.wiley.com/doi/10.1111/maps.13833 by Cochrane France, Wiley Online Library on [20/08/2025]. See the Terms and Conditions (https://onlinelibrary.wiley.com/terms-and-conditions) on Wiley Online Library for rules of use; OA articles are governed by the applicable Creative Commons License

lines, and east–west tie lines spaced at 4 km. Standard reductions were applied for both data sets, including parallax, daytime variation, and International Geomagnetic Reference Field removals for magnetic data; for gamma ray data, background and Compton effect removal were carried out, and leveling and microleveling were applied for both data sets. The gamma ray grid was generated using the minimum curvature method, and the magnetic grid using the bidirectional method, both with a cell size of 125 m.

Fieldwork, Sampling, and Petrography

In September 2019, WUR and MARV visited the area for a cursory investigation. It was possible to collect a first suite of samples from many of the field study sites indicated in Fig. 3c. Sample numbers (see also Tables SM-1 and SM-2 in supporting information) correspond to location numbers. Note that site 45 could not be plotted onto Fig. 3c, as no coordinates are available. Additional geological information was provided by Mauricio Borges (MB), who had visited the structure several times with students between 1989 and 1994.

Polished thin sections for all available samples from the NC structure were prepared at the Museum für Naturkunde, Berlin, Germany. Besides a detailed optical microscopic study of all 35 polished thin sections (results summarized in Table SM-1), three of these (NC-21b, NC-28, and NC-44), which showed abundant shock metamorphic features in optical microscopy, were further investigated using a four-axis universal stage (U-stage; Emmons, 1943) at the University of Vienna, Austria. Crystallographic orientations of planar fractures (PFs) and planar deformation features (PDFs) in quartz grains were measured by U-stage microscope, following the methods described by Engelhardt and Bertsch (1969), Stöffler and Langenhorst (1994), and Ferrière et al. (2009). The indexing of PDF sets was done using the manual graphical method: The orientation of the poles perpendicular to planes of PF/PDF and the optic axes of each host quartz grain were plotted by hand on a stereographic Wulff net and then indexed with Miller–Bravais indices, using the stereographic projection template (NSPT) of Ferrière et al. (2009). It should be noted that because it is impossible to uniquely distinguish between $\{10\bar{1}4\}$ and $\{10\bar{1}3\}$ orientations using the U-stage, when the angle between c-axis and poles to PDF is about 18–23°, all measured planes that fall into the overlap zone between $\{10\bar{1}4\}$ and $\{10\bar{1}3\}$ orientations are considered $\{10\bar{1}3\}$ orientations, as recommended by Ferrière et al. (2009).

Because most measured grains contain only one set of PF, and/or are oriented parallel to c(0001), as is also the case for a number of PDFs, they are not strictly speaking "indexed." However, the standard procedure has been to index these sets as well, to allow comparisons (see e.g., Ferrière et al., 2009; Holm-Alwmark et al., 2018).

RESULTS

Topographic/Morphological Analysis

The TanDEM-X topographic image of Fig. 1 shows the already confirmed Serra da Cangalha (13.7 km diameter) and Riachão (4.1 km diameter) impact structures, as well as the Nova Colinas structure. Serra da Cangalha stands out prominently with its well-defined rim structure and the inner "collar" around the central depression of the central uplift. The comparatively smaller and more eroded Riachão structure is less prominent. It is characterized by a weakly visible rim structure that is open to the northwest (Mazivieiro et al., 2013).

Nova Colinas (Fig. 3a and 3b), in the far northeast of the regional scene of Fig. 1, is located just south of some prominent tabular hill features. The structure itself comprises some subdued landforms in its outer parts, as well as a small (approximately 0.8 km wide) near-central elevation. The structure is seemingly transected into a northern and a southern sector by a west–east trending quasilinear structural element. The apparent central elevation of NC is further enhanced in the DEM of Fig. 3a, which reveals the west–east trending feature as a stream (the Macapá stream) that exploits radial cuts through the outer rim feature. Figures 3a and 3c also accentuate the elevation in the innermost part of the structure (described in Fig. 3b as a fault-dissected hill complex). Otherwise, much of the interior of the structure has subdued topography, whereas along its perimeter, elevations are more significant. The prominent plateau to the northwest of the structure denotes rocks more resistant to erosion, which could be attributed to the volcanics/subvolcanics of the Mosquito Formation that are extensively overlain by Corda Formation sedimentary strata, as also suggested by the radiometric and magnetic data (see Figs. 5a, 5b, and 6a, 6b), but field verification is required. Our ground-based research (cf. Fig. 3b) focused on the eastern and southeastern portions of the area, where sandstones of the Sambaíba Formation outcrop, which is relatively less resistant to erosion and, consequently, lacks significant elevations. Microdeformation features were found in these sedimentary rocks (Table SM-1; see Fig. 8).

The following description is based on the photogeological interpretation of the image of Fig. 3a

19455100, 2022, 8, Downloaded from https://onlinelibrary.wiley.com/doi/10.1111/maps.13833 by Cochrane France, Wiley Online Library on [20/08/2025]. See the Terms and Conditions (https://onlinelibrary.wiley.com/terms-and-conditions) on Wiley Online Library for rules of use; OA articles are governed by the applicable Creative Commons License

and MB's field records. Four relief patterns can be distinguished:

1. A linear to curvilinear hill pattern occurs in the outermost rim zone of the structure (Fig. 3b). The rim is marked by elongated shapes with sharp crests, sometimes with broad undulations that resemble open folds.
2. A symmetrical hill pattern is indicated by flat-topped hills arranged as discontinuous belts. These tabular hills occur inside the rim and are oriented along one of the inner annular structures. These hills are often dissected, have moderate elevations and high declivity slopes, and sometimes occur between ravines.
3. A dissected hill pattern occurs as a single relief unit arranged slightly offset from the center of the structure toward the south and elongated along north–south. This terrain has relatively enhanced amplitude and very dissected slopes.
4. A broad hill pattern with low amplitude and low declivity occurs in the north-central and northern parts of the structure. It is formed by broad, low-slope, and slightly convex hills with smooth surfaces that slope gently toward the course of the Macapá River. These hills are locally covered by cerrado vegetation and, in some parts, by bamboo. They exhibit a low-density drainage texture. In the field, they show extensive development of sandy, quartzose soil, which may represent colluvium.

Among the four topographic profiles extracted from the TanDEM-X DEM (profile orientations indicated in Fig. 3a; topographic profiles shown in Fig. SM-3d), the east–west profile particularly emphasizes the south-central elevation that is recognizable in the other profiles as well. The disrupted nature of this central elevation is obvious. The complex ridge and valley structures in the outer (rim) section of the structure are also well displayed in all four profiles (compare between the 10 and 20 km marks). The topography outside of the structure is much more prominent, from the east through to the northwest side, whereas the south/southeast side has been subject to enhanced degradation and is characterized by much subdued topography. Clearly, the Mosquito volcanics/subvolcanics toward the north have been more resistant to erosion than the sedimentary strata in the central and southern sectors.

Litho-Structural Analysis from Satellite Imagery

Two groups of structures can be distinguished in satellite image analysis (Figs. 3a and 8). The first group is related to the presence of annular, often concentric shapes, marked by structural lines that are probably

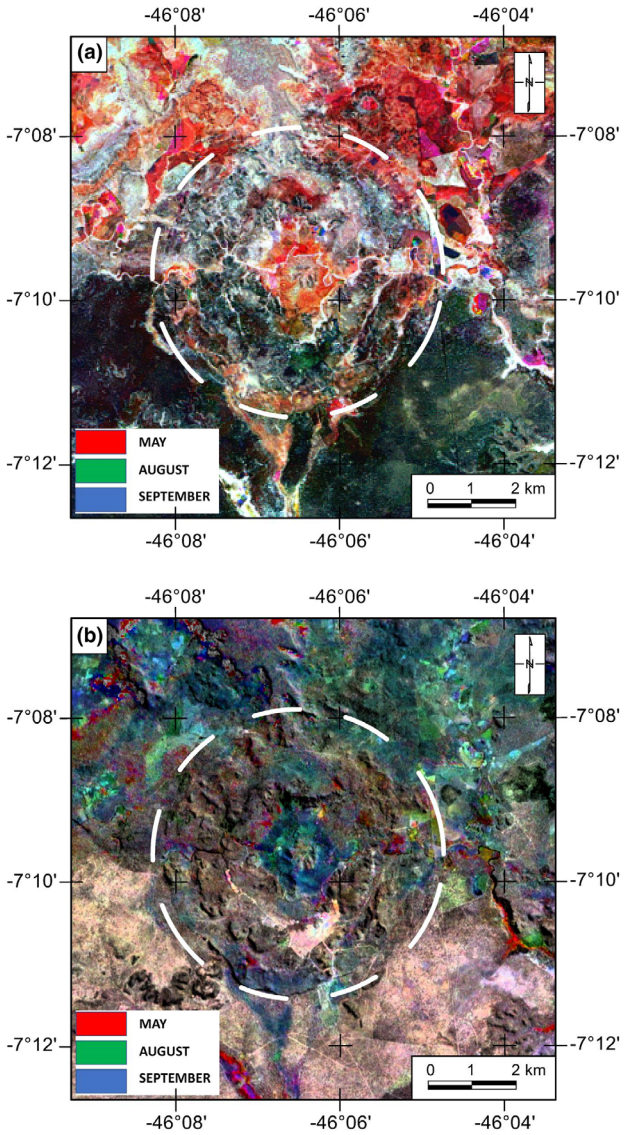

Fig. 4. a) The Color composite of multitemporal NDWI imagery built with 835 nm and 1650 nm spectral bands from the Landsat/ETM+ sensor. High NDWI responses signify high leaf water content. Images acquired on May 14, 2000 are in the red channel; thus, the red pixels mean that there is more leaf water content on this image. Likewise, the August 18, 2000 image is in the green channel, and the data taken on September 1, 1999 are in the blue channel, showing the regions/months with more leaf water content. For example, in the annular ring basin area, the pixels indicate high leaf water content during May. b) Landsat/ETM+ thermal band color composite for the same dates as in (a) and using the same color rendering. These images show the surface emissivity in the thermal infrared, which is related to canopy temperature. Thus, the innermost area, predominantly in blue, indicates a higher temperature in September. Note that the areas in blue in this figure coincide with those in red in (a), which supports the validity of the data. Also note that the possible central uplift area has a different behavior from that of the immediately surrounding annular area. The scale bar applies to both images. (Color figure can be viewed at wileyonlinelibrary.com.)

19455100, 2022, 8, Downloaded from https://onlinelibrary.wiley.com/doi/10.1111/maps.13833 by Cochrane France, Wiley Online Library on [20/08/2025]. See the Terms and Conditions (https://onlinelibrary.wiley.com/terms-and-conditions) on Wiley Online Library for rules of use; OA articles are governed by the applicable Creative Commons License

related to bedding strike, deformed primary structures, and the orientation of lithologies that appear dismembered, sometimes suggesting elongated shapes but with local constrictions. These elongations are likely related to strike orientations of deformation zones. This group of structures is fundamental in defining the architecture of the structure's annular forms (rings). These structures have circular to slightly elliptic trends. Planar lineaments often have centripetal orientation.

The second group of interpreted structures is related to brittle deformation superposed onto the first group. It defines faults and fractures of different types:

1. A set of tenuous structures with radial orientations has little lateral continuity and is dominated by short straight segments with lengths between 0.5 and 0.75 km.
2. A north/northwest–south/southeast to north/northeast–south/southwest striking set of lineaments coincides with the orientation of the regional Tocantins–Araguaia Lineament (Cordani et al., 2009). The individual structures are 0.5 to about 1.5 km long but can reach a maximum length of 2.7 km. The structures are spaced at <0.1 to 0.5 km. The features of this north–south trend are mainly bundled threefold, with one concentration at the center of the structure, where it marks its uplifted portion. The two other concentrations of north–south structures are present in the western and eastern parts of the NC structure. The relief over the structure is substantially dissected in areas where this group of lineaments is dominant.
3. A northeast–southwest trend is present throughout the entire structure but most common in the southeast and outermost northwest sectors. It may coincide with the trend of the Transbrasiliano Lineament (Cordani et al., 2009). These features occur with a high density of straight, short elements. Their lengths range from <0.25 to 1.2 km, and spacing can vary from <0.1 to 0.3 km.
4. A northwest–southeast set has discontinuous features that are widely spaced at 0.3–0.75 km. Their lengths range from 0.6 to 1.5 km. They project from the center of the structure toward the southwest sector. This structural orientation coincides with the Picos-Santa Ines trend (Cunha, 1986).
5. There is an east–west oriented structural element that bisects the impact structure. This strong structure controls the course of the Macapá stream. To the south of the structure, the Permian–Triassic units of the Parnaiba Basin seem to dominate (Klein & Souza, 2012). To the north, strata of the Jurassic–Cretaceous Mosquito and Corda formations may still occur within the structure. This east–west structural orientation, in part, coincides with the trend of the Xambioá-Teresina Arch (Aguiar, 1971, p. 120), which represents an important uplift area in the Parnaíba Basin. As the latest uplift activity has been attributed to the Cretaceous (Góes, 1995; Souza & Moreton, 2001), this trend association may, however, not provide an age constraint for the east–west structural feature. It cannot be excluded that this east–west structure was activated repeatedly, with only terminal activity represented by the Xambioá–Teresina Arch.

The Geobotanical Approach

Considering the soil and vegetation cover, lithological information from satellite imagery is indirectly and tentatively obtained via the geobotanical method described in the Methods section. Figure 4a depicts the NDWI color images of May 14, 2000 in red; of August 18, 2000 in green; and of September 1, 1999 in blue. Figure 4b exhibits the color composite of the thermal band of Landsat/ETM+ for the same dates and using the same color rendition as in Fig. 4a. Colors in both images indicate the seasonal variability in leaf water content, which in the NDWI color image (Fig. 4a) expresses greenness versus dryness, and in the TIR color image (Fig. 4b) expresses high versus low temperatures at different times. Vegetation temperatures increase with dryness, because of the absence of evapotranspiration by water stress.

In Fig. 4a, the annular zone surrounding the central hills appears red, indicating high leaf water content in May, right before the drought sets in, with pixels in orange indicating vegetation species in which the leaf water contents had decreased in August. In the September data, there are no blue pixels within the NC structure, meaning that, in September, there was hardly any water in the leaves. The areas in white indicate no differences in leaf water contents among the three dates, corresponding to the areas of riparian vegetation (evergreen). The areas in black/dark gray, which cover the southern half of the figure including some patches in the southern half of the NC structure, indicate an absence of significant green vegetation for the three data acquisition times.

Figure 4b shows for the annular zone surrounding the central hills a dominance of blue, indicating high temperatures in the September thermal data. The bright, white areas indicate high temperatures throughout the sampled period and refer to exposed soil, likely comprising sand of a small area with well-laminated arenite quarried for production of building stone (see Figs. SM-7g and SM-7h in supporting information). Pixels in red indicate higher temperatures in May, whereas pixels in yellow or orange indicate higher

19455100, 2022, 8, Downloaded from https://onlinelibrary.wiley.com/doi/10.1111/maps.13833 by Cochrane France, Wiley Online Library on [20/08/2025]. See the Terms and Conditions (https://onlinelibrary.wiley.com/terms-and-conditions) on Wiley Online Library for rules of use; OA articles are governed by the applicable Creative Commons License

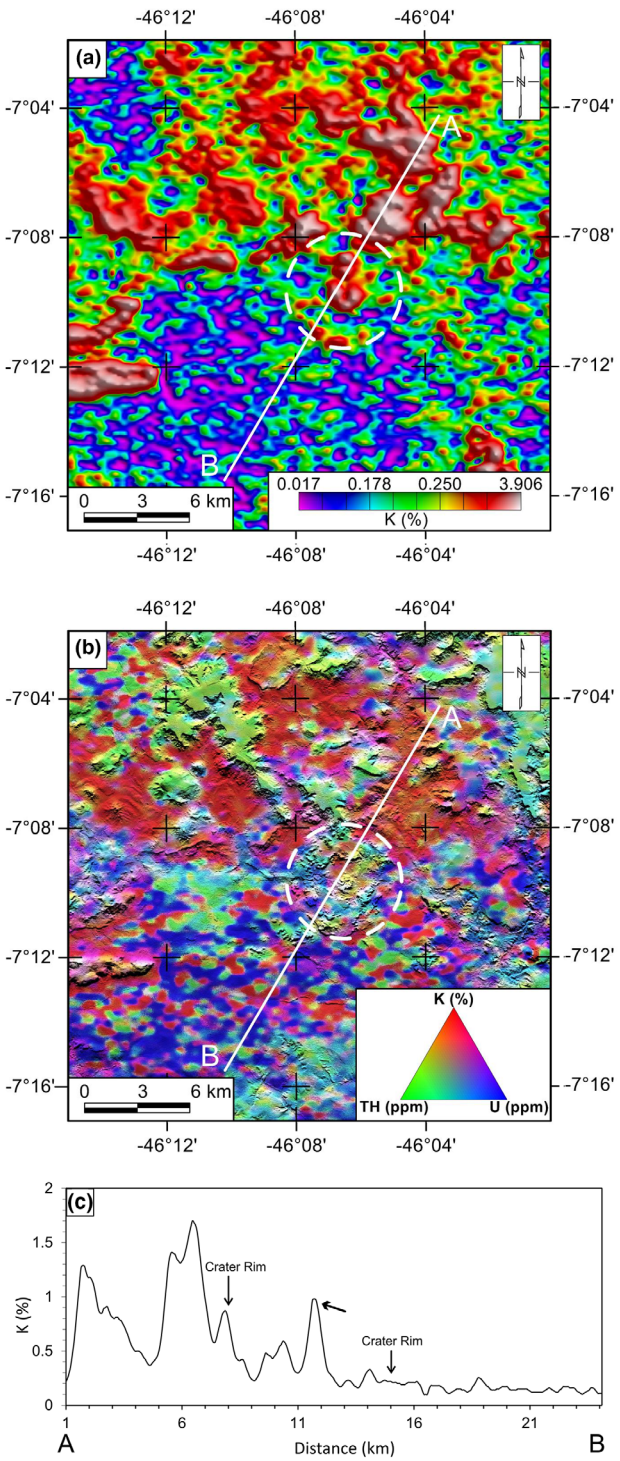

Fig. 5. Gamma ray data over the area of the Nova Colinas structure and surrounding terrain. a) Potassium channel depicting a positive anomaly around the center of the NC structure. b) RGB color composite of potassium, thorium, and uranium channels draped onto a DEM acquired by the TanDEM-X mission. c) A–B profile across the Nova Colinas structure showing elevation and potassium values along the profile. The fat arrow indicates the potassium peak at the center of the NC structure. (Color figure can be viewed at wileyonlinelibrary.com.)

temperatures in May and August. Pixels in green indicate higher temperatures in August, cyan in August and September, and those in blue indicate higher temperatures in September. These color variations in Fig. 4a and 4b reflect the phenological variability of the vegetation, showing variations in the floristic composition and seasonal behavior employed here as proxies for the underlying lithologies. The spatial coincidence in the innermost ring of the red and the blue pixels of these two images suggests a peculiar functioning of vegetation covers, probably associated with a similar lithological composition for the bedrock underneath. This is particularly remarkable for the area surrounding the central hills of the NC structure, but also in restricted areas near the rim, as well in the northwest, north, and northeast areas of the structure, where the Mosquito Formation likely occurs.

Geophysical Analysis

Analysis of geophysical data was carried out with specific processing techniques aimed at highlighting the lithological and morphological/structural characteristics of the NC structure. Figure 5a shows the K map and Fig. 5b the ternary RGB map of the potassium (K), thorium (Th), and uranium (U) channels, draped over a DEM. The gamma ray data provide a general view of the main lithotypes in the NC structure and its surroundings. The north and west areas of the structure present locally high concentrations of K in the surface-near material (Fig. 5a). According to the geological map (Fig. 2a), this region would be underlain by volcanic rocks of the Mosquito Formation, mainly basalt and mafic dikes. Plateau-like areas in this terrane are seemingly enriched in Th, and these areas have been mapped as covered by sedimentary rocks of the Corda Formation (Fig. 2a). Within the domains of the NC structure, the K channel presents a characteristic, pear-shaped, high concentration area over the center of the structure (Fig. 5a), coincident with an enrichment in Th. When combined with the TanDEM-X DEM, the high concentrations of K and Th delineate a near-circular area around the center (red and yellow in Fig. 5b). The A–B profile of Fig. 5c was extracted along the northeast–southwest direction across the structure, showing that the rim of the NC structure is characterized by low K values at the southwest, and medium/high values at the northeast, rim. A potassium-rich area is evident near the center of the structure, with a notable displacement in relation to the topographic peak (Fig. 5c) along the profile.

The magnetic data (Fig. 6a) were processed to obtain the analytical signal (Fig. 6b) and the tilt angle (Fig. 6c) images, as well as the power spectrum, which provides information about the outer limit of the

19455100, 2022, 8, Downloaded from https://onlinelibrary.wiley.com/doi/10.1111/maps.13833 by Cochrane France, Wiley Online Library on [20/08/2025]. See the Terms and Conditions (https://onlinelibrary.wiley.com/terms-and-conditions) on Wiley Online Library for rules of use; OA articles are governed by the applicable Creative Commons License

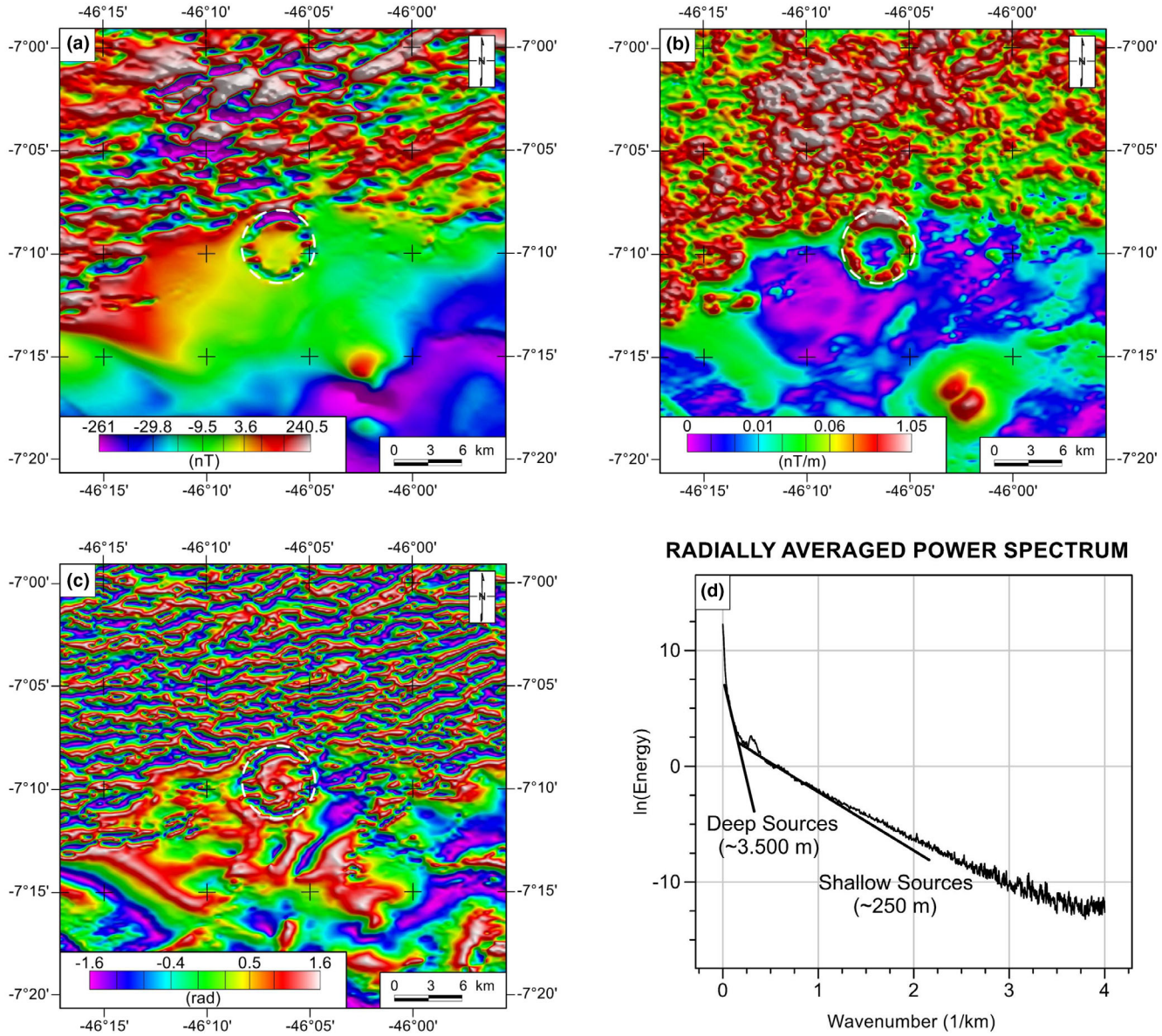

Fig. 6. Aeromagnetic data for the Nova Colinas impact structure and surrounding terrain. a) Total magnetic field image. b) Analytical signal of the magnetic field image. c) Tilt angle image. d) Power spectrum of the magnetic field, indicating the presence of two magnetic sources (see text for interpretation). The outer limit of the NC structure at 3.5 km radial distance from the center is suggested by the magnetic ring anomaly and topographic observations from TanDEM-X data. (Color figure can be viewed at wileyonlinelibrary.com.)

structure and the depth of the magnetic sources (Fig. 6d). The magnetic data show contrasting signatures between the area to the north of NC (coinciding with high K concentrations) and the one to the south (Fig. 6a–c). The northern area indicates short wavelength anomalies, ~1 km-wide and roughly aligned along northeast–southwest, which could correspond to basic volcanics and dikes of the Mosquito Formation (Fig. 6a). A circular magnetic anomaly with the same intensity appears over the NC structure. With the analytical signal, these anomalies are enhanced, and the occurrence of highly magnetic rocks in a concentric pattern of ~6–7 km diameter is emphasized (Fig. 6b). This might suggest that the outermost ring represents basalt spills, which would make sense in a bull's eye–type structure. This basalt hypothesis does presume that the Mosquito Formation actually transgressed into the area of the NC structure prior to impact. However, it has not been possible yet to determine the age of the impact, and, furthermore, our first ground truthing inside the crater found only sandstone outcrops of varying degrees of deformation.

19455100, 2022, 8, Downloaded from https://onlinelibrary.wiley.com/doi/10.1111/maps.13833 by Cochrane France, Wiley Online Library on [20/08/2025]. See the Terms and Conditions (https://onlinelibrary.wiley.com/terms-and-conditions) on Wiley Online Library for rules of use; OA articles are governed by the applicable Creative Commons License

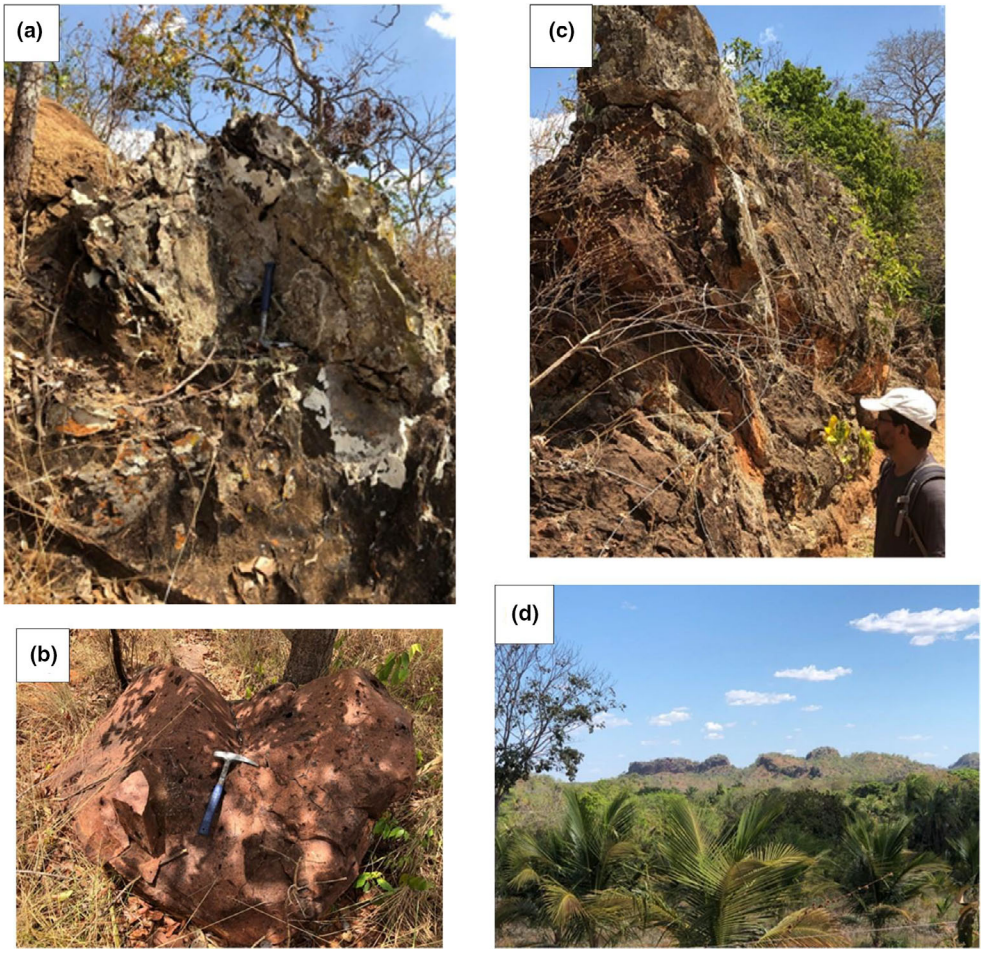

Fig. 7. Selected field impressions from the Nova Colinas structure. a) Looking at the hinge section of a meter scale (hammer for scale approximately 40 cm long), vertical, isoclinal fold in arenite. b) Field expression of a fresh specimen of the sedimentary breccia from site 32 with strongly silicified matrix and sedimentary clasts (see Table SM-1 for some petrographic information on sample 32). This sample is derived from an apparent breccia dike within the southeastern area outside the assumed central uplift. c) Radial arenite ridge with upright fold. d) Gentle, open folding along the northern outer edge of the central complex. View from the southeastern side of Fazenda do Nem (location indicated in caption to Fig. 3c). (Color figure can be viewed at wileyonlinelibrary.com.)

The tilt angle technique also indicates the presence of a magnetic ring feature along the rim of the structure, with a diameter of approximately 7 km. This anomaly is also shown by the analytical signal (Fig. 6c). The results obtained from the analysis of the power spectrum (Fig. 6d) indicate the existence of two magnetic sources, a shallow one at 250 m, and a deeper source at ~3500 m, depth.

First Field Observations

According to de Oliveira (2017), about 30% of the terrain of the structure is covered by dense riparian forest (especially along streams), 25% by cerrado, and the remainder is subject to agricultural use (pasture and cultivation). Because of the densely overgrown east–west corridor along the Macapá drainage, access to the innermost part of the structure from the northern side is difficult. Otherwise, the structure is generally covered by open vegetation—either grassland or quite open cerrado. Especially in the northern and southeastern interior, soil cover is extensive, with occasional remnant bedrock outcrops. Some of these exposures display folding at the meter scale (Fig. 7a). Note that the supporting information contains more field images, denoted SM-Fig. 7x. Throughout the interior of the structure, only arenites were encountered, sometimes sandy and then very friable, sometimes silicified and weathering resistant. The central elevated area comprises individual hills or tor-like structures (Fig. 7b). In the northern outer sector of the structure, to the north of Fazenda do Nem (see caption to Fig. 3c), the

19455100, 2022, 8, Downloaded from https://onlinelibrary.wiley.com/doi/10.1111/maps.13833 by Cochrane France, Wiley Online Library on [20/08/2025]. See the Terms and Conditions (https://onlinelibrary.wiley.com/terms-and-conditions) on Wiley Online Library for rules of use; OA articles are governed by the applicable Creative Commons License

strata are strongly fractured and display variable bedding orientation, from locally subhorizontal to steeply upturned (Fig. 7c). Figure 7d gives a view from the north onto the innermost hilly terrane, which is partly densely forested.

A number of dirt roads transect both the interior and the exterior of the structure. In the south, outside of the central complex, there are some prominent outcrops of strongly deformed (fractured) arenite (Fig. SM-7a). Also, in the southeast, outside of the central complex (location 32, Fig. 3c), a breccia was encountered in the form of an apparent meter-wide and some 10 meter-long dike, delineated on the surface by meter-sized blocks. This rock (Fig. 7b) is composed of a fine-grained, quartz-dominated matrix, with up to several centimeter-sized arenitic clasts of different color and grain size. Initially considered a possible polymict impact breccia, thin section analysis indicated that this is a strongly silicified sedimentary breccia with variably rounded to angular sedimentary clasts, none of which displayed any shock evidence (Table SM-1, sample 32). In the southeastern outer sector, a flat outcrop in the dirt road suggests the presence of monomict sandstone breccia (Fig. SM-7f in supporting information). A long, radially oriented outcrop of arenite showed an upright, isoclinal fold structure (Fig. 7c)—reminiscent of a "radial transpression ridge" of complex impact structures (Kenkmann et al., 2014; Kenkmann & von Dalwigk, 2000).

In the southern part of the central complex, a valley with ripple-marked, horizontally disposed and strongly laminated sandstone was encountered that is locally quarried on Fazenda Curral Velho (Figs. SM-7g and SM-7h). de Oliveira (2017) suggested this sandstone to belong to an intercalation in the Mosquito Formation—the Macapá Member.

A low but steep hill on the western side of the central elevation exposes intensively silicified and locally brecciated sandstone (Fig. SM-7i). Inside the central complex, rock deformation is highly variable. Locally, only mild fracturing with subcentimeter displacement on bedding planes may occur, or massive blocks of tens of meters dimension may be verticalized and locally folded. Along the northern outer side of the central complex, open folds with amplitudes of meters to tens of meters are noted (Fig. 7d). Bedding orientations determined at several sampling sites (cf. Fig. 3c) indicate strong deviation inside the structure from subhorizontal attitudes, with most dip angles >40 and up to 80 degrees. Bedding strike is also highly variable. Clearly, the sedimentary strata inside the structure were subject to considerable deformation at varied scales (millimeter to centimeter, to tens of meters).

Table 1. Shock deformation features in selected impact metamorphosed samples.

Sample no.	NC-21a	NC-21c	NC-28	NC-44
Q + 1 set of PF	266	280	209	130
Q + 2 sets of PF	94	59	97	30
Q + 3 sets of PF	4	2	n.d.	1
Q + 1 set of FF	8	10	2	18
Q + 1 FF + 1 PF	n.d.	2	n.d.	n.d.
Q + 1 FF + 2 PF	4	2	n.d.	2
Q + 1 set of PDF	26	7	14	19
Q + 2 sets of PDF	13	5	2	1
Q + 3 sets of PDF	7	n.d.	n.d.	1
Q + 1 PDF + 1 PF	16	8	4	5
Q + 1 PDF + 1 PF + 1 FF	n.d.	n.d.	n.d.	1
Q + 1 PDF + 2 PF + 1 FF	n.d.	n.d.	n.d.	1
Q + 1 PDF + 2 PF	11	3	n.d.	3
Q + 1 PDF + 3 PF	2	n.d.	n.d.	1
Q + 2 PDF + 1 PF	2	n.d.	n.d.	n.d.
Q + 3 PDF + 2 PF	n.d.	1	n.d.	n.d.
Total shocked grains	452	379	210	329
No. grains + PDF	77 (77)	24 (29)	30 (64)	23 (32)
With PDF in % of total	17	8.6	14.3	6
1 PF/2 PF	2.83	4.75	4.3	2.15

Observations were recorded in approximately one half of thin sections of standard size. In this area, all quartz grains were examined. Q = quartz; PF = planar fracture; FF = feather feature; PDF = planar deformation feature; n.d. = none detected; Numbers in brackets: No. of grains + PDF recalculated to the number for sample NC-21a = 451.

Outside of the structure, ridges are either table-topped, especially noted toward the northeast to northwest sides, or more irregularly shaped but still with mostly subhorizontal strata.

Petrography—Especially Shock Deformation

Of 32 specimens of various sandstones, collected at 27 outcrops mainly within, but also along the perceived margin of, the NC structure (Fig. 3c), 35 polished thin sections were prepared for optical microscopic analysis. Besides recording some general descriptive petrographic characteristics of these samples, all thin sections were screened—grain by grain—for possible evidence of impact diagnostic deformation. Table SM-1 provides a summary of these observations.

The NC sandstones have variable characteristics. The samples in hand are essentially quartz-dominated arenites, with the exception of sample 32 from the southeastern part of the structure. This sedimentary breccia carries a significant proportion of shale, quartzite, chert, and arenite clasts, which is not observed in the other samples. As sample 32 turned out to be entirely free of impact/shock deformation, it must be concluded that this

19455100, 2022, 8, Downloaded from https://onlinelibrary.wiley.com/doi/10.1111/maps.13833 by Cochrane France, Wiley Online Library on [20/08/2025]. See the Terms and Conditions (https://onlinelibrary.wiley.com/terms-and-conditions) on Wiley Online Library for rules of use; OA articles are governed by the applicable Creative Commons License

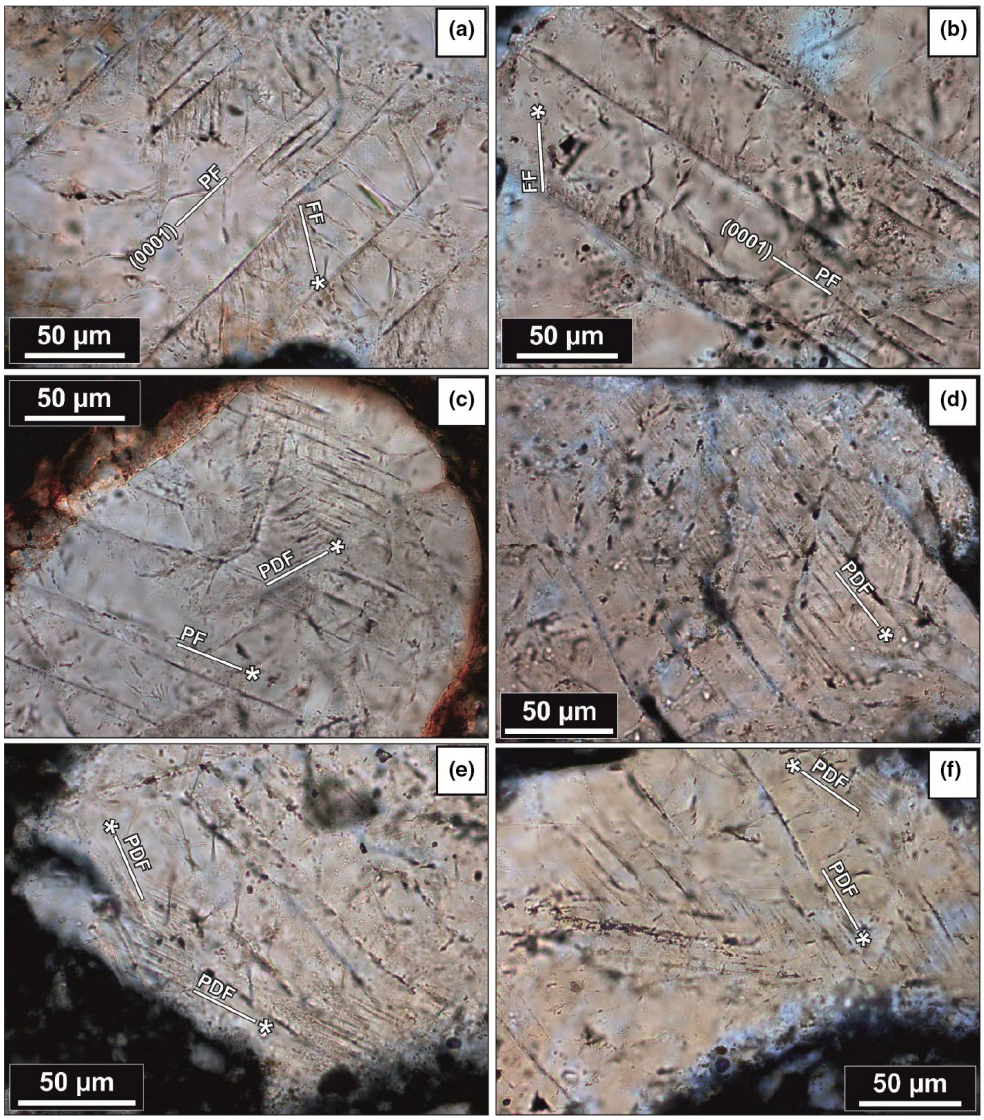

Fig. 8. Thin section photomicrographs of shocked quartz grains (all taken in cross-polarized light). a, b) Quartz grains with one set of PF with branched FFs (both in thin section NC-44). c) Quartz grains with one set of PFs and one set of PDFs (thin section NC-44). d) Quartz grain with one set of slightly decorated PDFs (thin section NC-28). e) Quartz grain with two sets of PDFs (thin section NC-28). f) Quartz grain with two sets of PDFs. One of the two sets is hardly visible on the upper right corner of the photomicrograph (thin section NC-28). Microstructure orientations are indicated only for the grains located in that area of the respective thin sections that is accessible with the U-stage assembly. Detailed results of the universal stage work are given in Tables 2 and 3. (Color figure can be viewed at wileyonlinelibrary.com.)

apparent dike feature could well be of sedimentary origin. It could have been generated as a "sand dike" through influx of sedimentary debris into an open fracture of up to more than 1 m width. The opening of this fracture, however, may have been a result of modification of the impact crater under extensional conditions.

Another important arenite lithology well represented in this sample suite typically displays a bimodal grain size distribution. Larger, often well-rounded quartz grains are embedded in a much finer grained quartz groundmass.

Many samples are characterized by variable amounts of splintery, highly angular quartz fragments in the comparatively finer size interval. In a significant number of these samples, it is also possible to identify concussion fractures between shattered but not yet dispersed quartz grains. Consequently, we interpret the splintery quartz fraction as derived from concussion fracturing and crushing, and this cataclasis as incipient formation of a monomict quartz/arenite breccia.

Table SM-1 also summarizes the observations related to shock deformation—namely observations of planar

19455100, 2022, 8, Downloaded from https://onlinelibrary.wiley.com/doi/10.1111/maps.13833 by Cochrane France, Wiley Online Library on [20/08/2025]. See the Terms and Conditions (https://onlinelibrary.wiley.com/terms-and-conditions) on Wiley Online Library for rules of use; OA articles are governed by the applicable Creative Commons License

fractures, feather features, and planar deformation features, besides undulous extinction and, locally, quartz mosaicism. Concussion fractures and reduction of porosity due to compaction were noted in a large number of samples (see Table SM-1). To date, no shock deformation has been observed in minor (feldspar) and accessory phases (e.g., zircon, apatite) in our samples.

In Fig. 3c, the symbols denoting sampling sites also represent different degrees of impact-related deformation. Four samples from three locations (#21a and c, 28, and 44) display significant degrees of shock deformation (see Table 1). These four samples are the only ones in our suite that demonstrated significant (not just rare) shock deformation (see Fig. 8a–f). All three sites are located within the structure, with site 44 in the central part where one might expect a remnant of a central uplift; sites 21a and 21c, approximately 50 m apart, about halfway out from the center; and site 28 not so far inward from the structure's rim section. The samples with strong cataclasis are exclusively derived from the outer part of the structure. This map (Fig. 3c) also demonstrates that, to date, only a part of the terrane inside of the structure has been studied and sampled. Samples with very little evidence of shock deformation are derived from the outer part of the structure. Sample 16 from outside the eastern rim does not show any diagnostic shock deformation but only spotwise occurring cataclasis. Based on optical microscopy, different types of planar microstructures (all of them crystallographically controlled) that characteristically form upon shock compression in

Table 2. Summary of PDF set abundances and indexed PDF crystallographic orientations in quartz grains from thin sections NC-28 and NC-44, as determined using the universal stage.

Sample No.	NC-28	NC-44
No. of investigated grains	28	17
No. of measured sets	48	25
No. of measured sets[a]	47	25
No. of sets/grain (N*)[a]	1.7	1.5
Relative abundance of PDF sets/grain (%)		
One set	46.4	58.8
Two sets	35.7	35.3
Three sets	17.9	5.9
Total	100	100
Indexed PDF crystallographic orientations; absolute frequency (%)[b]		
c (0001)	35.4	32.0
{10$\bar{1}$4}	8.3	n.d.
ω {10$\bar{1}$3}[c]	16.7	4.0
π {10$\bar{1}$2}	2.1	4.0
r, z {10$\bar{1}$1}	8.3	32.0
m {10$\bar{1}$0}	6.3	n.d.
ξ {11$\bar{2}$2}	8.3	12.0
s {11$\bar{2}$1}	4.2	8.0
ρ {21$\bar{3}$1}	n.d.	n.d.
x {51$\bar{6}$1}	6.3	n.d.
a {11$\bar{2}$0}	n.d.	n.d.
{22$\bar{4}$1}	n.d.	4.0
{31$\bar{4}$1}	n.d.	n.d.
t {40$\bar{4}$1}	2.1	n.d.
k {51$\bar{6}$0}	n.d.	4.0
Unindexed	2.1	n.d.
Total	100	100

n.d. = none detected.
[a]Calculated only on indexed sets (i.e., unindexed sets excluded).
[b]Method described in Engelhardt and Bertsch (1969).
[c]PDFs with measured orientations that plot in the overlapping zone between {10$\bar{1}$4} and {10$\bar{1}$3} were treated as {10$\bar{1}$3}. See Ferrière et al. (2009) for details.

Table 3. Summary of PF set abundances and indexed PF crystallographic orientations in quartz grains from thin sections NC-21b, NC-28, and NC-44, as determined using the universal stage.

Sample no.	NC-21b	NC-28	NC-44
No. of investigated grains	13	19	17
No. of measured sets	15	29	23
No. of measured sets[a]	15	25	23
No. of sets/grain (N)	1.2	1.5	1.4
No. of sets/grain (N*)[a]	1.2	1.3	1.4
Relative abundance of PF sets/grain (%)			
One set	84.6	57.9	76.5
Two sets	15.4	31.6	11.8
Three sets	n.d.	10.5	11.8
Total	100	100	100
Indexed PF crystallographic orientations; absolute frequency (%)[b]			
c (0001)	33.3	34.5	56.5
{10$\bar{1}$4}	n.d.	3.4	n.d.
ω {10$\bar{1}$3}[c]	6.7	n.d.	n.d.
π {10$\bar{1}$2}	6.7	n.d.	n.d.
r, z {10$\bar{1}$1}	13.3	24.1	13.0
m {10$\bar{1}$0}	6.7	3.4	n.d.
ξ {11$\bar{2}$2}	20.0	17.2	26.1
s {11$\bar{2}$1}	n.d.	3.4	n.d.
ρ {21$\bar{3}$1}	13.3	n.d.	n.d.
x {51$\bar{6}$1}	n.d.	n.d.	4.3
a {11$\bar{2}$0}	n.d.	n.d.	n.d.
{22$\bar{4}$1}	n.d.	n.d.	n.d.
{31$\bar{4}$1}	n.d.	n.d.	n.d.
t {40$\bar{4}$1}	n.d.	n.d.	n.d.
k {51$\bar{6}$0}	n.d.	n.d.	n.d.
Unindexed	n.d.	13.8	n.d.
Total	100	100	100

n.d. = none detected.
[a]Calculated only on indexed sets (i.e., unindexed sets excluded).
[b]Method described in Engelhardt and Bertsch (1969).
[c]PFs with measured orientations that plot in the overlapping zone between {10$\bar{1}$4} and ω{10$\bar{1}$3} were treated as {10$\bar{1}$3}. See Ferrière et al. (2009) for details.

19455100, 2022, 8, Downloaded from https://onlinelibrary.wiley.com/doi/10.1111/maps.13833 by Cochrane France, Wiley Online Library on [20/08/2025]. See the Terms and Conditions (https://onlinelibrary.wiley.com/terms-and-conditions) on Wiley Online Library for rules of use; OA articles are governed by the applicable Creative Commons License

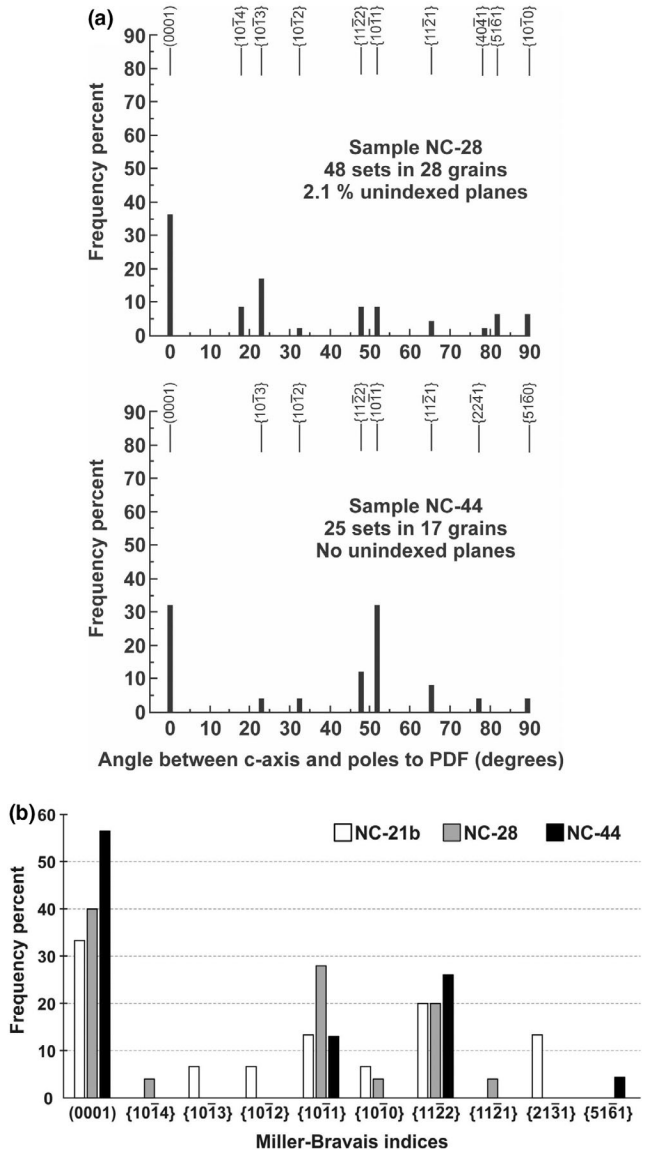

Fig. 9. a) Histogram of the absolute frequency percent of indexed PDFs (recalculated to 100% without unindexed PDF orientations) in quartz grains from thin sections NC-28 and NC-44, as determined following recommendations from Ferrière et al. (2009). Note that PDF planes that fall into the overlap zone between {10$\bar{1}$4} and {10$\bar{1}$3} crystallographic orientations are considered as {10$\bar{1}$3} orientations in this figure, as suggested by Ferrière et al. (2009). b) Histogram of the absolute frequency percent of indexed PFs (recalculated to 100% without unindexed PF orientations to allow consistent comparison of the data sets) in quartz grains from thin sections NC-21b, NC-28, and NC-44, as determined following recommendations from Ferrière et al. (2009).

quartz grains can be distinguished: PFs, feather features (FFs), and PDFs (e.g., Engelhardt & Bertsch, 1969; Ferrière & Osinski, 2013; French & Koeberl, 2010; Poelchau & Kenkmann, 2011; Stöffler & Langenhorst, 1994). PFs consist of open fractures with spacings in the range from 10 to 20 μm or more, whereas FFs are short, parallel to subparallel, closely spaced lamellae that branch off a PF. Both these types of microdeformation features form at relatively low pressures (~5–10 GPa, Poelchau & Kenkmann, 2011; Stöffler et al. [2018] and references therein). PDFs form at higher pressures (~10–30 GPa) and consist of thin (usually from a few 10s to ~200 nm thick), straight, planar lamellae of amorphous or high-dislocation-density material, forming parallel sets of features spaced 2–10 μm apart, and occurring at one or more crystallographic orientations per host grain.

Deformation effects in the four Nova Colinas samples with significant bona fide shock deformation range from quartz with one or more sets of PFs, presence of FFs (Fig. 8a), and of one to three sets of PDFs—with additional grains with combinations of these three types of deformation (see Table 1). Notably, sample 21a carries a rather high number of grains with PDFs (77 grains with PDFs were counted in a half thin section). The sample from site 28 contains much fewer quartz grains with PDFs but, when the grains with PDFs are compared against the total number of quartz grains, the proportion of 14.3% is nearly as high as that for the sample from site 21. In contrast, the sample from site 44 (likely on the central uplift) only has 6% of quartz grains that carry PDFs.

Typically, PFs (Fig. 8a and 8b) occur either as a single set per grain or together with one or more sets of PDFs. In some cases, thin lamellar features branch off PFs and then together form FFs (Fig. 8a and 8b). More rarely two (Fig. 8e and 8f), or up to three, sets of PDFs (also true for PFs, but even more rare) were observed under the U-stage (see Tables 2 and 3). Some of the PDFs are slightly decorated with tiny fluid inclusions (Fig. 8e).

The crystallographic orientations of 67 PF and 72 PDF sets in 74 shocked quartz grains from three thin sections were measured with the U-stage. Data (in absolute frequency percent) are reported in Tables 2 and 3 for PDFs and PFs, respectively (note that only two sets of PDF oriented parallel to the c(0001) and r{10$\bar{1}$1} orientations were measured in two quartz grains from thin section NC-21b, and, thus, are not reported in Table 2). Absolute frequency percent of indexed PDF sets versus angle between the c-axis and poles to PDF planes for samples NC-28 and NC-44 are shown in Fig. 9a. In both cases, PDF sets oriented parallel to the c(0001) orientation are most abundant, representing one-third of the measured PDF sets. In the case of sample NC-28, about 17 absolute frequency percent of the measured PDF sets are parallel to the ω{10$\bar{1}$3} orientation, whereas planes parallel to the {10$\bar{1}$4}, r {10$\bar{1}$1}, ξ{11$\bar{2}$2}, m{10$\bar{1}$0}, x{51$\bar{6}$1}, s{11$\bar{2}$1}, π{10$\bar{1}$2},

19455100, 2022, 8, Downloaded from https://onlinelibrary.wiley.com/doi/10.1111/maps.13833 by Cochrane France, Wiley Online Library on [20/08/2025]. See the Terms and Conditions (https://onlinelibrary.wiley.com/terms-and-conditions) on Wiley Online Library for rules of use; OA articles are governed by the applicable Creative Commons License

and t{40$\bar{4}$1} orientations are also present (Fig. 9a; see Table 2), but in lower proportions (i.e., less than 10 absolute frequency percent). In the case of sample NC-44, PDF sets parallel to the r{10$\bar{1}$1} orientation represent one-third of the measured PDF sets (i.e., as much as the basal sets), whereas 12 absolute frequency percent of the measured PDF sets are parallel to the ξ{11$\bar{2}$2} orientation, while planes parallel to the s{11$\bar{2}$1}, ω{10$\bar{1}$3}, π{10$\bar{1}$2}, {22$\bar{4}$1}, and k{51$\bar{6}$0} orientations occur in minor amounts, representing less than 10 absolute frequency percent (Fig. 9a; see Table 2). The number of PDF sets per quartz grain varies from one to three, with an average of 1.7 and 1.5 sets per grain for samples NC-28 and NC-44, respectively.

The absolute frequency percent of indexed PFs in quartz grains for samples NC-21b, NC-28, and NC-44 is shown in Fig. 9b. As in the case of the PDFs, a large proportion from one-third to more than half (i.e., about 57 absolute frequency percent for sample NC-44) of the PFs is oriented parallel to the c(0001) orientation. Planar fractures oriented parallel to the r{10$\bar{1}$1} and ξ{11$\bar{2}$2} orientations are also more or less abundant, representing from about 13 to 26 absolute frequency percent of the measured PF sets. A few PF sets are oriented parallel to the m{10$\bar{1}$0}, {21$\bar{3}$1}, ω{10$\bar{1}$3}, π{10$\bar{1}$2}, {10$\bar{1}$4}, s{11$\bar{2}$1}, and x{51$\bar{6}$1} orientations (Fig. 9b; see Table 3). As for the PDFs, the number of PF sets per quartz grain varies from one to three, with an average of 1.2–1.4 sets per grain (see Table 3).

DISCUSSION

We report the results of detailed analysis of the Nova Colinas structure. Our work has been focused on satellite image analysis and interpretation, geophysical studies of the regional and local magnetic and gamma spectroscopic anomalies, reconnaissance fieldwork, and shock petrographic studies. A first-order conclusion is that the Nova Colinas structure represents an impact structure, and this is supported by the results gained from all these data and methods (see below for detailed discussion).

Remote Sensing, Geophysics, and Fieldwork

The remote sensing-based geobotany data show the vegetation covers with a phenological–ecological variability that suggests, particularly for the central region of the structure, a bull's eye pattern typical of impact structures formed in a layered target. It is well known that, upon water stress, stomata close, thus decreasing evapotranspiration and increasing leaf temperature (Kimball & Bernacchi, 2006). The multitemporal thermal remote sensing data used in this research allow us to see indirectly the seasonal variability in the water status of vegetation.

Furthermore, Gerhards et al. (2016) showed that water stress is well measured on the basis of remotely sensed temperature indices, and that near-infrared/short-wave infrared (NIR/SWIR) reflectance-based indices (such as the NDWI) are related to plant water content. The availability of NIR and SWIR data in the sensor system applied here allowed the direct deduction of leaf water data via the NDWI index. Our approach is supported by independent data (surface temperature and reflected solar radiation) that supply information about a key ecological parameter, with which the variability in phenological and floristic behavior are associated. These responses are partially confirmed by gamma spectrometric data: throughout the central region—the innermost hills and the annular terrane around them—there is evidence for elevated K in the radiometric data (Fig. 5a). Significant differences in vegetation cover can be expected to be associated with varied concentrations of this element (for comparison, in the sparsely vegetated outer rim area, the radiometric K signal is comparatively low).

The analytical signal of the magnetic field (Fig. 5b), which may suggest the discontinuous presence of basalts in the outermost zone, finds some support in the leaf water image (Fig. 4a). There are some restricted areas with K anomalies coincident with areas of seasonal leaf water signature, like that found over the basalts to the north of the structure and in its innermost zone. We provisionally interpret the K anomaly over the central part of the Nova Colinas structure as the signal of a lower stratigraphic unit that became uplifted during the collapse and modification phase of cratering. Figure 6a–c exhibits a significant ring-shaped positive magnetic anomaly in the rim area around the structure, whereas the interior of the structure is entirely devoid of a magnetic signature. This annular anomaly defines a diameter of approximately 7 km, which suggests that the Nova Colinas impact structure is larger than the previous estimate of 5.5–6 km of Gottwald et al. (2020).

In the region surrounding the NC structure, a comparison between the K anomaly map (Fig. 5a and 5b) and the magnetic anomalies (Fig. 6a–c) shows a clear distinction between the areas to the north of the NC structure and the southern part of the structure and terrain to the south of it. The northern area, presumably underlain by basic volcanic or intrusive rocks of the Mosquito Formation, exhibits high K values and a set of low-wavelength, east/northeast–west/southwest-trending magnetic highs and lows. It is reasonable to assume that the areas with high K and

19455100, 2022, 8, Downloaded from https://onlinelibrary.wiley.com/doi/10.1111/maps.13833 by Cochrane France, Wiley Online Library on [20/08/2025]. See the Terms and Conditions (https://onlinelibrary.wiley.com/terms-and-conditions) on Wiley Online Library for rules of use; OA articles are governed by the applicable Creative Commons License

elevated Th to the north of the structure do not represent the Mosquito volcanics, but rather are indicative of the surficial deposits of Corda Formation sedimentary rock (see Rabelo et al. [2019] for more information on these strata). The area to the south exhibits low K values and high-wavelength magnetic highs and lows, with no clear spatial trend. The anomalies in this area are thought to correspond to the sandstones of the Sambaíba Formation. A possible U enrichment in this southern region may also be related to Sambaíba sandstone. There is also a remarkable magnetic dipole anomaly near the center of the southeast quadrant (Fig. 6a and 6b), at approximately 8–9 km from the NC structure, which disrupts the high-wavelength patterns of the magnetic signature of the Sambaíba sandstones (and perhaps older units of the Motuca and Pedra de Fogo formations). Considering the numerous basic dikes related to the Mosquito volcanism commonly found cutting the Sambaiba sandstones in this wider region (according to the regional geological map; CPRM, 2012), local anomalies may be interpreted as the signatures of near-surface mafic intrusions. Ground-based studies are required to test these preliminary interpretations of the geophysical signatures to the north of the structure and in its southern sectors. In particular, the relationships between K, Th, and U anomalies and sedimentary deposits in the various parts of the study area need to be followed up by handheld gamma spectrometric surveying.

The power spectrum of the magnetic data (Fig. 6d) shows two magnetic sources in the entire area depicted. One is located at approximately 3500 m depth and is possibly related to the top of the crystalline basement underneath the sedimentary strata of the Parnaíba Basin, in accordance with estimations by Milani and Thomaz (2000). The second, shallower source occurs at 250 m depth and could be related to mafic intrusive rocks possibly related to Mosquito (sub)volcanism.

Clearly, the field inspection of 2019 does not suffice to assess the geology and structure of the crater structure. Much more work needs to be done. However, several first-order observations can be made:

1. The structure comprises a rim zone of dismembered ridges in a curved (annular) and linear pattern. Our satellite image interpretation shows that complex faulting has affected the structure. A well-defined east–west trending structure transgresses the NC structure and exploits the bed of the Macapá stream (cf. Fig. 3b, where this east–west structural feature is interpreted as a Mesozoic–Cenozoic Fault Zone). If this feature could be dated, it might represent a constraint on the maximum age of impact (see the Age of the Nova Colinas Impact Structure section). However, a more regional analysis beyond the extent of the structure must be carried out in order to separate likely impact-generated lineaments (faults) from effects of regional tectonics.
2. So far, only arenitic strata have been observed throughout the structure, with the exception of a gritty, arenitic sedimentary rock (sample 32) that occurs in dike form and is strongly silicified—but entirely unshocked.
3. The northernmost sector of the structure (north of Fazenda do Nem) still must be examined for possible occurrence of Mosquito volcanics (cf. Fig. 3c for the location of this area).
4. Within the structure, folding is noted at decimeter to meter scales. In one location in the southwestern part of the structure, an at least 100 m long upright fold structure—in radial orientation with respect to the center of the structure—may represent a transpression ridge (see Kenkmann and von Dalwigk, 2000).
5. Samples from many sites revealed more or less intense cataclasis. Some of these samples are better denominated monomict impact breccia (Fig. SM-8f and Table SM-1 in supporting information).
6. The hills in the interior of the structure are characterized by highly variable and often steep bedding orientations. Further detailed structural analysis of this inner terrain is warranted. At this point, we assume that these hills represent an erosional remnant of an original central uplift structure (as to be expected for an impact structure of this size). This may be further supported by the observation that the innermost terrain has a significantly different radiometric signature (Fig. 5a–c) from the outer parts—possibly due to elevation of a K-Th-rich lithology toward the present surface.
7. One site (between locations 39 and 44; Fig. 7a), which was not sampled, is characterized by complete silicification at the "hill scale." Again, more regional investigation regarding hydrothermal overprint in the interior of the structure is still required.

Proof of Impact Deformation in Quartz

In four sandstone samples from the Nova Colinas structure, PFs, FFs, and PDFs in quartz grains were found in considerable numbers. In several other specimens, comparatively rare shock deformation was recorded (Table 1). We documented 72 PDF sets in 45 quartz grains using the U-stage (Tables 2 and 3). Because specific crystallographic orientations of PDFs are formed in different shock pressure regimes (see e.g., Hörz, 1968; Huffman & Reimold, 1996), shock pressure can be estimated using U-stage measurements of PDF orientations.

19455100, 2022, 8, Downloaded from https://onlinelibrary.wiley.com/doi/10.1111/maps.13833 by Cochrane France, Wiley Online Library on [20/08/2025]. See the Terms and Conditions (https://onlinelibrary.wiley.com/terms-and-conditions) on Wiley Online Library for rules of use; OA articles are governed by the applicable Creative Commons License

On the basis of our optical microscopic observations and U-stage results, we can, first of all, confirm that the Nova Colinas structure represents an impact structure—the ninth in the Brazilian impact record. Furthermore, our crystallographic results indicate that the investigated shocked samples have experienced weak to moderate shock levels. Sample NC-21b recorded the lowest level of shock (PFs and extremely rare PDFs; pressure approximately 5–10 GPa); sample NC-44 (with PDFs mainly oriented parallel to the c(0001) and {10$\bar{1}$1} orientations) experienced shock pressure between ~10 and 16 GPa; and finally, sample NC-28 (with PDFs mainly oriented parallel to the c(0001) and ω{10$\bar{1}$3} orientations) recorded shock pressure between 10 and 20 GPa. These pressure estimates are constrained by the minimum shock pressures of at least 16 and 20 GPa needed for the formation of PDF orientations parallel to ω{10$\bar{1}$3} and to π{10$\bar{1}$2}, respectively (see Hörz, 1968).

These results are somewhat surprising, as sample 28 was collected the furthest out from the center of the impact structure, and sample 44 in what is considered the remnant of the central uplift (cf. Fig. 3c). We only have three samples with shock pressure estimations, and the result may well reflect heterogeneity of shock pressure distribution, which is to be expected for complex impact structures with collapsed central uplifts. Such a skewed distribution of shock levels has also been demonstrated for the Cerro do Jarau structure in the Paraná Basin, Brazil, by Reimold et al. (2019). That no higher shock levels were identified (so far) for the innermost sector of the structure could hint at a significant amount of erosion for Nova Colinas.

Age of the Nova Colinas Impact Structure

Until now, no datable impact-generated material has been found in the structure, and again, this may be related to a likely significant degree of degradation of an old structure formed in supracrustal strata. The search for impact melt-bearing breccias will of course continue. Currently, the only age constraints for this impact event stem from the chronostratigraphic knowledge about this area. If the mafic volcanics of the Mosquito Formation extended at impact time into the area of the Nova Colinas structure, the age proposed for this formation of 199.7 ± 2.4 Ma (Merle et al., 2011) would provide a maximum impact age. If this extension of the Mosquito Formation into the structure was not the case, then the ages of the Permian to Triassic Sambaíba and Motuca formations would provide a maximum upper age limit for the impact, maybe as high as 250 Ma (e.g., Vaz et al., 2007). Therefore, the impact would be dated to the beginning of the Mesozoic, between the Middle Triassic and Lower Jurassic periods. Should it be possible to constrain the age of the prominent east–west trending structural zone, calibrated against regional knowledge, this might provide a further constraint on the age of impact. The key for further age constraints on the Nova Colinas impact may lie in the northern part of the structure with possible Mosquito Formation exposures.

CONCLUSIONS

This work represents a detailed multidisciplinary approach to the Nova Colinas structure in the southern part of the Parnaiba Basin in Maranhão State of northeastern Brazil. The following major conclusions can be drawn:

- On the basis of this discovery paper Nova Colinas is confirmed as the ninth impact structure of Brazil and the 11th known in South America. The Nova Colinas structure shows a distinct magnetic ring feature that suggests a diameter of the structure of the order of 7 km. This suggests that this clearly significantly eroded impact structure should have originally been of complex crater morphology.
- The structure is characterized by a strong K and a somewhat less intense Th radiometric signature over its interior.
- In a geobotanical approach, two sensitive parameters for vegetation cover in climates with severe droughts were analyzed in multispectral images: leaf water and canopy temperature for the periods at the beginning, middle, and end of the annual drought of 1999–2000. The phenological and floristic diversity indicated is partly spatially related to the gamma spectrometry and to a ring structure. These features are suggestive of a more complex local geology, particularly in the center of the structure. The phenological and floristic diversity indicated can be, in part, related to the gamma spectrometry, thus indicating a ring structure and reinforcing the hypothesis of different lithologies. The results, when analyzed in an integrated manner, provide further support for the hypothesis of a bull's eye–type structure commonly associated with an impact structure formed in sedimentary strata.
- Our preliminary field study has demonstrated that the interior of the eroded crater structure is characterized by significant macro- and mesoscopic structural deformation. Folding is prominent at the decimeter to meter scales. Cataclasis is noted in many places and confirmed by microscopy to be related to widespread monomict brecciation.
- A large number of arenite samples from the interior of the structure show strong microscopic evidence of shock deformation. Further work must focus on

19455100, 2022, 8, Downloaded from https://onlinelibrary.wiley.com/doi/10.1111/maps.13833 by Cochrane France, Wiley Online Library on [20/08/2025]. See the Terms and Conditions (https://onlinelibrary.wiley.com/terms-and-conditions) on Wiley Online Library for rules of use; OA articles are governed by the applicable Creative Commons License

more detailed field analysis and sampling of especially the hills in the southcentral area that represents remnants of the central uplift.
- Multiple arenite samples with prominent shock deformation in the form of planar fractures, feather features, and—above all—planar deformation features confirm the impact cratering origin of the Nova Colinas structure.
- Shock levels determined for three samples are <10, 10–16, and 10–20 GPa, respectively—that is, shock degrees are weak to moderate.
- Currently, the age of the Nova Colinas impact is only supported by a few stratigraphic considerations. Estimates range from Middle Triassic to Lower Jurassic, or younger.
- Much more work needs to be done on this newly confirmed impact structure, especially comprehensive geological mapping and further geophysical work, such as a comprehensive gravity investigation. Further sampling and continuation of the shock petrographic analysis are also required.

Acknowledgments—Hans Knöfler, formerly of the Museum für Naturkunde Berlin, is thanked for a great suite of polished thin sections, without which this shock petrographic study could not have been conducted. LF thanks Christian Koeberl for providing access to the universal stage at the University of Vienna and the Juranek-Yansouni Family for financial support. Marília Prado Freire (University of São Paulo) is thanked for assistance with the generation of the stratigraphic column of Fig. 2b. WUR and NH are grateful for partial support of this study from the Brazilian *Coordenação de Aperfeiçoamento de Pessoal de Nível Superior* (CAPES), under Finance Code 001. Their work has been supported by CNPq Bolsa de Produtividade grants No. 305761/2019-6 (to WUR), 309878/2019-5 (to NH), and # 302679/2018-9 (to APC). We are grateful to Associate Editor Michael Poelchau and two reviewers (an anonymous one and Thomas Kenkmann) for their detailed and analytical recommendations.

Data Availability Statement—Research data are not shared.

Editorial Handling—Dr. Michael Poelchau

REFERENCES

Abreu, F. A. M., Silva, J. M. R., Faria, Júnior L. E.C. Rodrigues, M. D. R., and Truckenbrodt, W. 1977. *Projeto Balsas. Relatório Final. Ministério das Minas e Energia*. Departamento Nacional da Produção Mineral. Convênio DNPM/UFPA, Belém, 47 pp.

Aguiar, G. A. 1971. Revisão geológica da Bacia Paleozóica do Maranhão. In *Congresso Brasileiro de Geologia 25, São Paulo, 1971, Anais da Sociedade Brasileiro de Geologia*, 3, 113–22.

Almeida, T. I. R., Juliani, C., Mantovani, W., and Pérez-Aguilar, A. 2007. Comunidades florestais como indicadores geobotânicos: o caso da mineralização aurífera do Grupo Serra do Itaberaba, Guarulhos, São Paulo. *Revista Brasileira de Geociências* 37: 37–49.

Almeida, T. I. R., do, Amaral, C. H., Botelho, M., Ribeiro, E. F., and Penatti, N. C. 2019. Geobotany in a Fault in the World's Largest Continuous Wetland in Central South America. *Wetlands Ecology and Management* 27: 171–85.

Andrade, L. S. 2019. *Paleoambiente e paleoclima da Formação Pedra de Fogo da Bacia do Parnaíba e sua correlação com os eventos globais de silicificação do Permiano*, 177 pp. Tese de Doutorado (unpublished), Universidade Federal de Pará, Belém.

Ballén, O. A. R., Goés, A. M., Negri, F., De Assis Maziviero, M. V., and do Santos Teixeira, V. Z. 2013. Sistema eólico úmido nas successões sedimentares interderrames da Formação Mosquito, Jurássico da Província Parnaíba, Brasil. *Brazilian Journal of Geology* 43: 695–710.

Barbosa da Silva, A. 2020. Identification of Impact Cratering-Related Similarities Based on Airborne Geophysical Data and Satellite Images: The Cabeça de Sapo Structure, Parnaiba Basin, Northeast Brasil. *Journal of the Geological Survey of Brazil* 3: 97–111.

Brenha, S. L. A. 2013. Identificação da cratera meteórica Cabeça de Sapo: Metamorfismo de choque em rochas sedimentares da maior estrutura de impacto do Estado de maranhão, Nordeste do Brasil. In: Encontro Nacional de Astronomia 16, Brasilia. https://www.16.enast.com.br/pt-br/br/o-evento/atividades/identificação-da-cratera-metoritica-cabeca-de-sapo-metamorf/. Accessed June 23, 2021.

Brito Neves, B. B., Fuck, R. A., Cordani, U. G., and Thomaz, A. F. 1984. Influence of Basement Structures on the Evolution of the Major Sedimentary Basins of Brazil: A Case of Tectonic Heritage. *Journal of Geodynamics* 1: 495–510.

Cordani, U. G., Neves, B. B. B., and Thomaz, F. A. 2009. Estudo preliminar de integração do Pré-Cambriano com os eventos tectônicos das bacias sedimentares brasileiras (Republicação). *Boletim de Geociências da Petrobrás* 17: 133–204.

CPRM. 2012. *Mapa geológico e de recursos mineraisdo estado de Maranhão*. Brasília: Serviço Geológico do Brasil—CPRM. http://rigeo.cprm.gov.br/doc/mapa_geologia.

Crósta, A. P., Reimold, W. U., Vasconcelos, M. A. R., Hauser, N., Oliveira, G. J. G., Mazivieiro, M. V., and Goés, A. M. 2019a. Impact Cratering: The South American Record—Part 1. *Chemie der Erde—Geochemistry* 79: 1–61.

Crósta, A. P., Reimold, W. U., Vasconcelos, M. A. R., Hauser, N., Oliveira, G. J. G., Mazivieiro, M. V., and Goés, A. M. 2019b. Impact Cratering: The South American Record—Part 2. *Chemie der Erde—Geochemistry* 79: 191–220.

Cunha, F. M. B. 1986. Evolução Paleozóica da Bacia do Parnaíba e Seu Arcabouço Tectônico. Universidade Federal do Rio de Janeiro, Instituto de Geociências, Dissertação de Mestrado, 107 pp.

Eiten, G. 1994. Vegetação do Cerrado. In *Cerrado: Caracterização, Ocupação e Perspectivas*, edited by M. N. Pinto, 17–73. Brasília: Universidade de Brasília.

Emmons, R. C. 1943. *The Universal Stage (with Five Axes of Rotation)*. New York: Geological Society of America.

19455100, 2022, 8, Downloaded from https://onlinelibrary.wiley.com/doi/10.1111/maps.13833 by Cochrane France, Wiley Online Library on [20/08/2025]. See the Terms and Conditions (https://onlinelibrary.wiley.com/terms-and-conditions) on Wiley Online Library for rules of use; OA articles are governed by the applicable Creative Commons License

Engelhardt, W. V. and Bertsch, W. 1969. Shock Induced Planar Deformation Structures in Quartz from the Ries Crater, Germany. *Contributions to Mineralogy and Petrology* 20: 203–34.

Ferreira, M. A. 2013. *Bacia de Parnaíba*. In: Seminário Técnico-Ambiental da 12ª Rodada de Licitações de Petróleo e Gás, 19 setembro, Rio de Janeiro. http://rodadas.anp.gov.br/arquivos/Round12/Seninarios_R12/apresentacao/r12_04_parnaiba.pdf/.

Ferrière, L. and Osinski, G. R. 2013. Shock Metamorphism. In *Impact Cratering: Processes and Products*, edited by G. R. Osinski, and E. Pierazzo, 106–24. Chichester, UK: Blackwell Publishing Ltd.

Ferrière, L., Morrow, J. R., Amgaa, T., and Koeberl, C. 2009. Systematic Study of Universal-Stage Measurements of Planar Deformation Features in Shocked Quartz: Implications for Statistical Significance and Representation of Results. *Meteoritics & Planetary Science* 44: 925–40.

French, B. M. and Koeberl, C. 2010. The Convincing Identification of Terrestrial Meteorite Impact Structures: What Works, What Doesn't, and Why. *Earth-Science Reviews* 98: 123–70.

Gao, B.-C. 1996. NDWI—A Normalized Difference Water Index for Remote Sensing of Vegetation Liquid Water from Space. *Remote Sensing of Environment* 58: 257–66.

Gerhards, M., Rock, G., Schlerf, M., and Udelhoven, T. 2016. Water Stress Detection in Potato Plants Using Leaf Temperature, Emissivity, and Reflectance. *International Journal of Applied Earth Observation and Geoinformation* 53: 27–39.

Góes, A. M. 1995. *A Formação Poti (Carbonífero Inferior) da Bacia do Parnaíba*. Tese (Doutorado), Universidade de São Paulo, Instituto de Geociências. https://doi.org/10.11606/T.44.1995.tde-11022014-105309.

Góes, A. M. O. and Feijó, F. J. 1994. Bacia de Parnaíba. *Boletim de Geociências da Petrobrás* 8: 57–67.

Gottwald, M., Fritz, T., Breit, H., Schättler, B., and Harris, A. 2017. Remote Sensing of Terrestrial Impact Craters: The TanDEM-X Digital Elevation Model. *Meteoritics & Planetary Science* 52: 1412–27.

Gottwald, M., Kenkmann, T., and Reimold, W. U. 2020. *Terrestrial Impact Structures, The TanDEM-X Atlas, Part 1 and 2*. Munich: Verlag Dr. Friedrich Pfeil.

Gottwald, M., Kenkmann, T., Reimold, W. U., Fritz, T., and Breit, H. 2021. The TanDEM-X Digital Elevation Model and Terrestrial Impact Structures. *IEEE Journal of Selected Topics in Applied Earth Observations and Remote Sensing* 14: 4128–38.

Hörz, F. 1968. Statistical Measurements of Deformation Structures and Refractive Indices in Experimentally Shock Loaded Quartz. In *Shock Metamorphism of Natural Materials*, edited by B. M. French, and N. M. Short, 243–53. Baltimore, Maryland: Mono Book Corporation.

Holm-Alwmark, S., Ferrière, L., Alwmark, C., and Poelchau, M. H. 2018. Estimating Average Shock Pressures Recorded by Impactite Samples Based on Universal Stage Investigations of Planar Deformation Features in Quartz—Sources of Error and Recommendations. *Meteoritics & Planetary Science* 53: 110–30.

Huffman, A. R. and Reimold, W. U. 1996. Experimental Constraints on Shock-Induced Microstructures in Naturally Deformed Silicates. *Tectonophysics* 256: 165–217.

Instituto Brasileiro de Geologia e Estatística (IBGE). 2011. *Mapa Geológico do Estado do Maranhão, scale 1 : 1,400,000*. Equipe de Geologia da Gerência de Recursos Naturais (GRN) do IBGE no Estado do Pará.

Kenkmann, T. 2021. The Terrestrial Impact Crater Record: A Statistical Analysis of Morphologies, Structures, Ages, Lithologies, and More. *Meteoritics & Planetary Science* 56: 1024–70.

Kenkmann, T. and von Dalwigk, I. 2000. Radial Transpression Ridges: A New Structural Feature of Complex Impact Craters. *Meteoritics & Planetary Science* 35: 1189–201.

Kenkmann, T., Vasconcelos, M. A. R., Crósta, A. P., and Reimold, W. U. 2011. The Complex Impact Structure Serra da Cangalha, Tocantins State, Brazil. *Meteoritics & Planetary Science* 46: 875–89.

Kenkmann, T., Poelchau, M. H., and Wulf, G. 2014. Structural Geology of Impact Craters. *Journal of Structural Geology* 62: 156–82.

Kimball, B. A. and Bernacchi, C. J. 2006. Evapotranspiration, Canopy Temperature, and Plant Water Relations. In *Managed Ecosystems and CO_2*, edited by J. Nosberger, S. P. Long, R. J. Norby, M. Stitt, G. R. Hendrey, and H. Blum, Ecological Studies Series, vol. 187, 311–24. Berlin: Springer Publishers, 456 p.

Klein, E. L. and Souza, C. S. 2012. *Geologia e recursos minerais do Estado do Maranhão: Sistema de Informações Geográficas – SIG: texto explicativo dos mapas geológicas e de recursos minerais do Estado do Maranhão. Escala 1:750,000*. Belém: Serviço Geológico do Brasil – CPRM. https://rigeo.cprm.gov.br/xmlui/handle/doc/17861?show=full.

Lima, M. I. C. 1995. Metodologia de Interpretação Radargeológica: Exemplo da Sinéclise do Parnaíba e de Seu Embasamento. Tese de Doutorado (unpublished), Universidade Federal de Pará, Belém, 283 pp.

Marques, R. P., Kassab, F., Jr, Molina, E. C., and Andrade, F. A. R. 2006. *Levantamentos aerogeofísicos para a identificação de áreas com ocorrência potencial de petróleo e gás na Bacia do Parnaíba—Tomo II, área Parnaíba—Aerolevantamento magnético e gamaespectrométrico*. São Paulo: Report Convênio ANP—USP, 109 pp.

Marzoli, A., Callegaro, S., Dal Corso, J., Davies, J. H. F. L., Chiaradia, M., Youbi, N., Bertrand, H., et al. 2018. The Central Atlantic Magmatic Province (CAMP): A Review. In *The Late Triassic World*, edited by L. H. Tanner, Topics in Geobiology 46, Chapter 4, 91–125. Cham: Springer.

Mazivieiro, M. V., Vasconcelos, M. A. R., Crósta, A. P., Goés, A. M., Reimold, W. U., and Carneiro, C. C. 2013. Geology and Impact Features of Riachão Structure, Northern Brazil. *Meteoritics & Planetary Science* 48: 2044–58.

Merle, R., Marzoli, A., Bertrand, H., Reisberg, L., Verati, C., Zimmermann, C., Chiaradia, M., et al. 2011. $^{40}Ar/^{39}Ar$ ages and Sr–Nd–Pb–Os geochemistry of CAMP tholeiites from Western Maranhão basin (NE Brazil). *Lithos* 122: 137–51.

Milani, E. J. and Thomaz, F. A. 2000. Sedimentary Basins of South America. In *Tectonic Evolution of South America*, edited by U. G. Cordani, E. J. Milani, A. T. Filho, and D. A. Campos, 389–449. Rio de Janeiro: 31st IGC.

Nogueira, A. C. R., Rabelo, C. E. N., Góes, A. M., Cardoso, A. R., Bandeira, J., Rezende, G. L., Santos, R. F., et al. 2021. Evolution of Jurassic Intertrap Deposits in the Parnaíba Basin, Northern Brazil: The Last Sediment-Lava

19455100, 2022, 8, Downloaded from https://onlinelibrary.wiley.com/doi/10.1111/maps.13833 by Cochrane France, Wiley Online Library on [20/08/2025]. See the Terms and Conditions (https://onlinelibrary.wiley.com/terms-and-conditions) on Wiley Online Library for rules of use; OA articles are governed by the applicable Creative Commons License

Interaction Linked to the CAMP in West Gondwana. *Palaeogeography Palaeoclimatology Palaeoecology* 572: 110370. https://doi.org/10.1016/j.palaeo.2021.110370.
de Oliveira, A. 2017. Perspectiva do potencial geoparque do astroblema Cabeça de Sapo no município de Novas Colinas. MA. M.Sc. dissertation, Centro de Ciências Sociais Aplicadas, Universidade Estadual do Maranhão, São Luis. www.ppdsr.uema.br/wp-content/uploads/2018/08/andreia-de-oliveira.pdf.
Oliveira, A. L., Pimentel, M. M., Fuck, R. A., and Oliveira, D. C. 2018. Petrology of Jurassic and Cretaceous Basaltic Formations from the Parnaíba Basin, NE Brazil: Correlations and Associations with Large Igneous Provinces. In *Cratonic Basin Formation: A Case Study of the Parnaíba Basin of Brazil*, edited by M. C. Daly, R. A. Fuck, J. Julià, D. I. M. Macdonald, and A. B. Watts, 279–308. London: Geological Society London Special Publications, 472. https://doi.org/10.1144/SP472.21.
Poelchau, M. H. and Kenkmann, T. 2011. Feather Features: A Low-Shock-Pressure Indicator in Quartz. *Journal of Geophysical Research* 116: B02201. https://doi.org/10.1029/2010JB007803.
Rabelo, C. E. N., Cardoso, A. R., Nogueira, A. C. R., Soares, J. L., and Góes, A. M. 2019. Genesis of Poikilotopic Zeolite in Aeolianites: An Example from the Parnaíba Basin, NE Brazil. *Sedimentary Geology* 385: 61–78. https://doi.org/10.1016/j.sedgeo.2019.03.013.
Reimold, W. U., Crósta, A. P., Hasch, M., Kowitz, A., Hauser, N., Sanchez, J. P., Amarante Simões, L. S., et al. 2019. Shock Deformation Confirms the Impact Origin for the Cerro do Jarau, Rio Grande do Sul, Brazil, Structure. *Meteoritics & Planetary Science* 54: 2384–97.
Santos, M. E. C. M. and Carvalho, M. S. S. 2009. *Paleontologia das Bacias do Parnaiba, Grajaú e São Luiz*. Brasília: CPRM, 215 pp.
Schmieder, M. and Kring, D. A. 2020. Earth's Impact Events Through Geologic Time: A List of Recommended Ages for Terrestrial Impact Structures and Deposits. *Astrobiology* 20: 91–141. https://doi.org/10.1089/ast.2019.2085.
Souza, J. O. and Moreton, L. C. 2001. Programa Levantamentos Geológicos Básicos do Brasil. – PLGB. Xambioá – Folha SB.22-Z-B. Estados da Pará e Tocantins. Escala 1:250,000, CPRM/DIEDIG/DEPAT, Brasília. 45 pp.
Stöffler, D., Hamann, C., and Metzler, K. 2018. Shock Metamorphism of Planetary Silicate Rocks and Sediments: Proposal for an Updated Classification System. *Meteoritics & Planetary Science* 53: 5–49.
Stöffler, D. and Langenhorst, F. 1994. Shock Metamorphism of Quartz in Nature and Experiment: I. Basic Observation and Theory. *Meteoritics & Planetary Science* 29: 155–81.
Tuomisto, H., Ruokolainen, K., and Yli-Halla, M. 2003. Dispersal, Environment, and Floristic Variation of Western Amazonian Forests. *Science* 299: 241–4.
Vasconcelos, M. A. R., Crósta, A. P., and Molina, E. C. 2010. Geophysical Characteristics of Four Possible Impact Structures in the Parnaíba Basin, Brazil: Comparison and Implications. In *Large Meteorite Impacts and Planetary Evolution IV*, edited by R. L., Gibson, and W. U. Reimold, 201–17. GSA Special Paper 465. Boulder, Colorado: Geological Society of America.
Vasconcelos, M. A. R., Crósta, A. P., Reimold, W. U., Goes, A. M., Kenkmann, T., and Poelchau, M. H. 2013. The Serra da Cangalha Impact Structure, Brazil: Geological, Stratigraphic and Petrographic Aspects of a Recently Confirmed Impact Structure. *Journal of South American Earth Sciences* 45: 316–30.
Vaz, P. T., Rezende, N. G. A. M., Wanderley, F. J. R., and Travassos, W. A. S. 2007. Bacia do Parnaiba. *Boletim de Geociências da Petrobrás* 15: 253–63.

SUPPORTING INFORMATION

Additional supporting information may be found in the online version of this article.

Table SM-1. Some characteristics of the Nova Colinas sample suite. Note that it was not possible to obtain samples from all field study sites indicated in Fig. 3c. PF—planar fracture; FF—feather feature; PDF—planar deformation feature; sst—sandstone; GM—groundmass; *n x PDF* = number of quartz grains with PDF.

Table SM-2. List of GPS coordinates (in decimal values) for all sampled study sites in the Nova Colinas impact structure. Locations are shown in Fig. 3c (in degree/minute values). All listed data are in the form "Longitude S, Latitude W." Bedding orientations determined at some of these sites are also listed.

Figure SM-3d. The four topographic profiles that were extracted from the TanDEM-X digital elevation model (DEM) shown in Fig. 3a. See text for detail.

Figures SM-7x. Field impressions from Nova Colinas: (SM-7a) View toward the north of the structure, where a table-topped ridge can be discerned. (SM-7b) Tor-like erosion features of arenite along the N edge of the central elevation (view toward the south). Strata are steeply upturned. (SM-7c) Steeply upturned and possibly slightly folded arenite NW of Fazenda do Nem. This block is approximately 2 m high. View onto an outer sandstone ridge in the environs of the northern, inner grassland. (Fig. SM-7d) View from the N across Fazenda do Nem onto the morphologically more interesting central complex. (SM-7e) Large outcrops of strongly fractured arenite along the southern periphery of the central complex. (SM-7f) Intense fracturing in arenite, suggesting the presence of monomict breccia. (SM-7g) Exposure of ripple-marked, well-laminated sandstone in the southeastern interior of the structure. (SM-7h) Well-laminated sandstone, of the type shown in Fig. SM-7g, prepared for industrial purposes. (SM-7i) Intensely silicified and brecciated arenite at the southwestern edge of the central complex (remnant of central uplift).

19455100, 2022, 8, Downloaded from https://onlinelibrary.wiley.com/doi/10.1111/maps.13833 by Cochrane France, Wiley Online Library on [20/08/2025]. See the Terms and Conditions (https://onlinelibrary.wiley.com/terms-and-conditions) on Wiley Online Library for rules of use; OA articles are governed by the applicable Creative Commons License